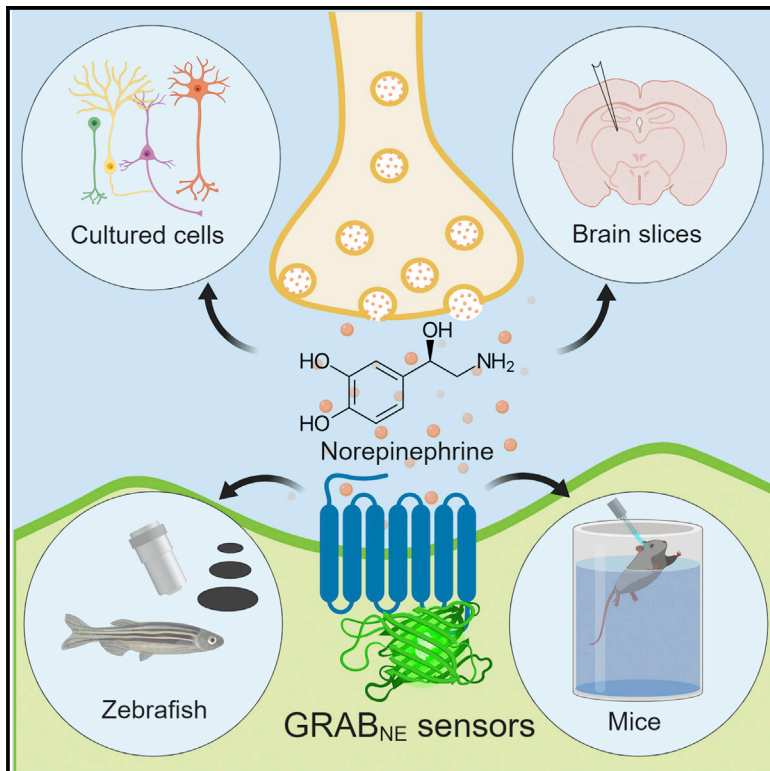


Neuron

A Genetically Encoded Fluorescent Sensor for Rapid and Specific *In Vivo* Detection of Norepinephrine

Graphical Abstract



Authors

Jiesi Feng, Changmei Zhang,
Julieta E. Lischinsky, ..., Dayu Lin,
Jiulin Du, Yulong Li

Correspondence

yulongli@pku.edu.cn

In Brief

Feng et al. develop and validate a pair of genetically encoded GPCR-activation-based norepinephrine sensors, which, for the first time, enable specific *in vivo* measurement of norepinephrine dynamics during stressful behaviors with high spatiotemporal resolution in zebrafish and mice.

Highlights

- GRAB_{NE} sensors are genetically encoded GPCR activation-based norepinephrine sensors
- GRAB_{NE} distinguishes norepinephrine from dopamine with 1,000-fold specificity
- The norepinephrine measurements are sensitive, with high spatiotemporal resolution
- Norepinephrine dynamics are observed during stressful behaviors in zebrafish and mice



A Genetically Encoded Fluorescent Sensor for Rapid and Specific *In Vivo* Detection of Norepinephrine

Jiesi Feng,^{1,2,3} Changmei Zhang,^{5,9} Julieta E. Lischinsky,⁶ Miao Jing,^{1,2,3,4} Jingheng Zhou,⁷ Huan Wang,^{1,2} Yajun Zhang,^{1,3,8} Ao Dong,^{1,2,3} Zhaofa Wu,^{1,2} Hao Wu,^{1,2,13} Weiyu Chen,^{5,9} Peng Zhang,⁸ Jing Zou,¹² S. Andrew Hires,¹² J. Julius Zhu,^{8,14,15,16} Guohong Cui,⁷ Dayu Lin,^{6,10,11} Jiulin Du,^{5,9} and Yulong Li^{1,2,3,4,17,*}

¹State Key Laboratory of Membrane Biology, Peking University School of Life Sciences, Beijing 100871, China

²PKU-IDG/McGovern Institute for Brain Research, Beijing 100871, China

³Peking-Tsinghua Center for Life Sciences, Academy for Advanced Interdisciplinary Studies, Peking University, Beijing 100871, China

⁴Chinese Institute for Brain Research, Beijing 100871, China

⁵Institute of Neuroscience, State Key Laboratory of Neuroscience, CAS Center for Excellence in Brain Science and Intelligence Technology, Chinese Academy of Sciences, Shanghai 200031, China

⁶Neuroscience Institute, New York University School of Medicine, New York, NY 10016, USA

⁷Neurobiology Laboratory, National Institute of Environmental Health Sciences, NIH, Research Triangle Park, NC 27709, USA

⁸Department of Pharmacology, University of Virginia School of Medicine, Charlottesville, VA 22908, USA

⁹University of Chinese Academy of Sciences, Beijing 100049, China

¹⁰Department of Psychiatry, New York University School of Medicine, New York, NY 10016, USA

¹¹Center for Neural Science, New York University, New York, NY 10016, USA

¹²Department of Biological Sciences, Neurobiology Section, University of Southern California, Los Angeles, CA 90089, USA

¹³School of Life Sciences, Tsinghua University, Beijing 100084, China

¹⁴School of Medicine, Ningbo University, Ningbo 315010, China

¹⁵Donders Institute for Brain, Cognition and Behavior, Radboud University Nijmegen, 6525 Nijmegen, the Netherlands

¹⁶Department of Physiology, School of Basic Medicine, Tongji Medical College, Huazhong University of Science and Technology, Wuhan 430030, China

¹⁷Lead Contact

*Correspondence: yulongli@pku.edu.cn

<https://doi.org/10.1016/j.neuron.2019.02.037>

SUMMARY

Norepinephrine (NE) is a key biogenic monoamine neurotransmitter involved in a wide range of physiological processes. However, its precise dynamics and regulation remain poorly characterized, in part due to limitations of available techniques for measuring NE *in vivo*. Here, we developed a family of GPCR activation-based NE (GRAB_{NE}) sensors with a 230% peak $\Delta F/F_0$ response to NE, good photostability, nanomolar-to-micromolar sensitivities, sub-second kinetics, and high specificity. Viral- or transgenic-mediated expression of GRAB_{NE} sensors was able to detect electrical-stimulation-evoked NE release in the locus coeruleus (LC) of mouse brain slices, looming-evoked NE release in the midbrain of live zebrafish, as well as optogenetically and behaviorally triggered NE release in the LC and hypothalamus of freely moving mice. Thus, GRAB_{NE} sensors are robust tools for rapid and specific monitoring of *in vivo* NE transmission in both physiological and pathological processes.

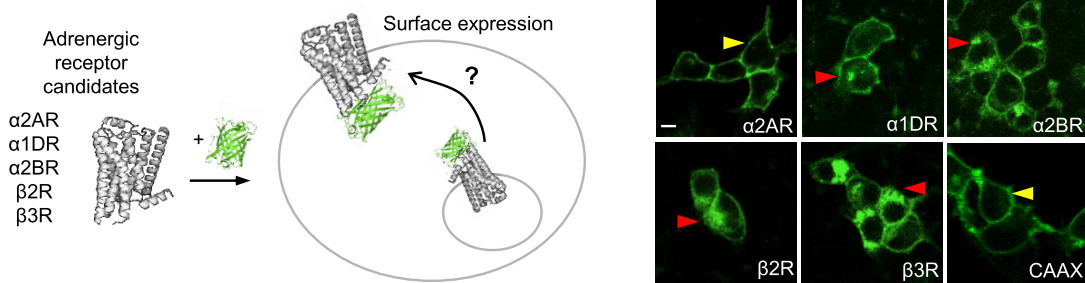
INTRODUCTION

Norepinephrine (NE) is a key monoamine neurotransmitter in the central nervous systems and peripheral organs of vertebrate organisms. It plays important roles in a plethora of physiological processes, allowing the organism to cope with its ever-changing internal and external environments. In the brain, NE is synthesized primarily in neurons of the locus coeruleus (LC), a small yet powerful nucleus located in the pons. Noradrenergic LC neurons project throughout the brain and exert a wide range of effects, including processing sensory information (Berridge and Waterhouse, 2003), regulating the sleep-wake or arousal state (Berridge et al., 2012), and mediating attentional function (Bast et al., 2018). Blocking noradrenergic transmission causes impaired cognition and arousal and is closely correlated with a variety of psychiatric conditions and neurodegenerative diseases, including stress (Chrousos, 2009), anxiety (Goddard et al., 2010), depression (Moret and Briley, 2011), attention-deficit hyperactivity disorder (ADHD) (Berridge and Spencer, 2016), and Parkinson's disease (PD) (Espay et al., 2014). In the sympathetic nervous system, NE plays critical roles, such as regulating heart function (Brodde et al., 2001) and blood pressure (Zimmerman, 1981).

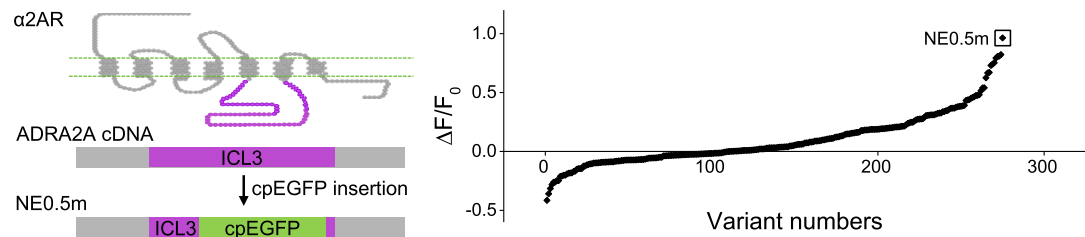
Despite its clear importance in a wide range of physiological processes, the spatial and temporal dynamics of NE in complex



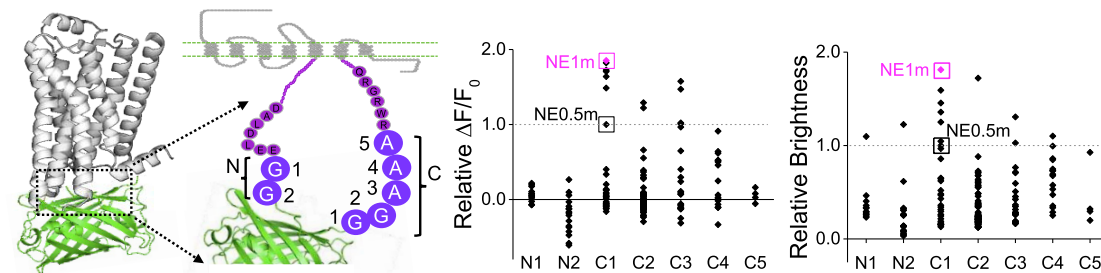
A Selection of NE sensitive GPCR



B Insertion sites screening



C Optimization of coupling linkers



D Affinity tuning of NE sensors

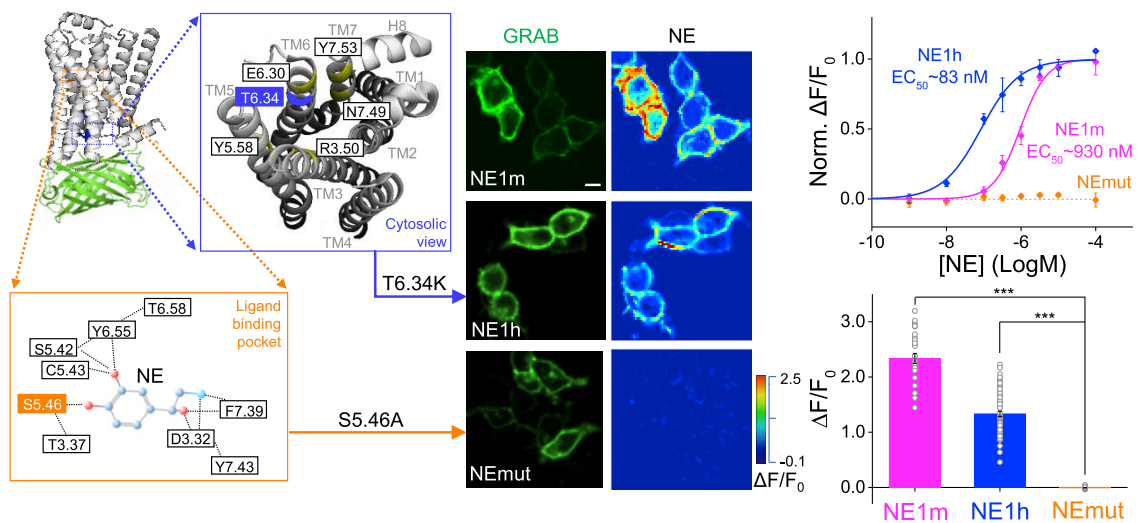


Figure 1. Design and Optimization of Genetically Encoded NE Sensors

(A) Selection of a candidate sensor scaffold by screening several NE-binding GPCRs. Shown at the right are example images of the indicated chimeric GPCR-cpEGFP candidates expressed in HEK293T cells. Yellow arrows indicate robust membrane trafficking, and red arrows indicate impaired membrane trafficking. See also Figure S1.

(B) Identification of the most responsive NE sensor, NE0.5m (indicated by the black square), by screening the cpEGFP insertion sites in ICL3 of the α 2AR. $\Delta F/F_0$ refers to the peak change in fluorescence intensity in response to 100 μ M NE.

(legend continued on next page)

organs (e.g., the vertebrate brain) are poorly understood at the *in vivo* level due to limitations associated with current detection methods. Classic detection methods, such as microdialysis-coupled biochemical analysis (Bito et al., 1966; Justice, 1993; Watson et al., 2006), have low temporal resolution (typically 5 min/collection) and complex sampling procedures, limiting the ability to accurately measure the dynamics of noradrenergic activity in the physiological state (Chefer et al., 2009). Recent improvements in microdialysis—in particular, the introduction of the nano-LC-microdialysis method (Lee et al., 2008; Olive et al., 2000)—have significantly increased detection sensitivity; however, the sampling rate is still on the order of minutes. Electrochemical detection techniques, including fast-scan cyclic voltammetry (FSCV) based on measuring currents generated by the oxidation of NE (Bruns, 2004; Park et al., 2009; Robinson et al., 2008; Zhou and Misler, 1995), provide nanomolar sensitivity and millisecond temporal resolution; however, their inability to distinguish NE from other monoamine neurotransmitters—particularly dopamine (Robinson et al., 2003)—presents a significant physiological limitation for measuring noradrenergic transmission both in *ex vivo* tissue preparations and *in vivo*. Both microdialysis-based and electrochemical techniques detect volume-averaged NE levels in the extracellular fluid and therefore cannot provide cell-type-specific or subcellular information.

Real-time imaging of NE dynamics would provide an ideal means to non-invasively track NE with high spatiotemporal resolution. A recent innovation in real-time imaging, cell-based neurotransmitter fluorescent engineered receptors (CNiFERS) (Muller et al., 2014) convert an extracellular NE signal into an intracellular calcium signal that can be measured using fluorescence imaging. However, CNiFERS require implantation of exogenous tumor cell lines and can report only volume transmission of NE. By contrast, genetically encoded sensors could, in theory, circumvent the above-mentioned limitations to provide fast, clear, non-invasive, and cell-type-specific reporting of NE dynamics. In practice, genetically encoded NE sensors developed to date either have poor signal-to-noise ratio and narrow dynamic range (e.g., a <10% change in fluorescence resonance energy transfer [FRET] ratio under optimal conditions) or lack *in vivo* characterization (Nakanishi et al., 2006; Patriarchi et al., 2018; Vilardaga et al., 2003; Wang et al., 2018b), thus limiting their applicability *in vivo*.

To overcome these limitations, we developed a series of genetically encoded single-wavelength fluorescent GPCR activation-based NE (GRAB_{NE}) sensors with rapid kinetics, a $\Delta F/F_0$ dynamic range of $\sim 200\%$, and EGFP-comparable spectra, brightness, and photostability. Here, we showcase the wide applicability of our GRAB_{NE} sensors using a number of *in vitro*

and *in vivo* preparations. In every application tested, the GRAB_{NE} sensors readily reported robust and chemical-specific NE signals. Thus, our GRAB_{NE} sensors provide a powerful imaging-based probe for measuring the cell-specific regulation of noradrenergic transmission under a wide range of physiological and pathological conditions.

RESULTS

Development and Characterization of GRAB_{NE} Sensors

Inspired by the structure (Rasmussen et al., 2011a, 2011b) and working mechanism (Chung et al., 2011; Manglik et al., 2015; Nygaard et al., 2013) of the β_2 adrenergic G-protein-coupled receptor (GPCR), we exploited the conformational change between the fifth and sixth transmembrane domains (TM5 and TM6, respectively) upon ligand binding to modulate the brightness of an attached fluorescent protein. Building upon the successful strategy of generating GPCR activation-based sensors for acetylcholine (GACH) (Jing et al., 2018) and dopamine (dLight and GRAB_{DA}; Patriarchi et al., 2018; Sun et al., 2018), we first screened human adrenergic receptors for a potential scaffold. We inserted circularly permuted EGFP (cpEGFP) into the third intracellular loop domain (ICL3) of three α -adrenergic receptors (α_1 DR, α_2 AR, and α_2 BR) and two β -adrenergic receptors (β_2 R and β_3 R; Figure 1A). Among these five constructs, α_2 AR-cpEGFP had the best membrane trafficking, indicated by its high colocalization ratio with membrane-targeted RFP (Figure S1); we therefore selected this receptor as the scaffold for further development.

The length and amino acid composition of the linkers surrounding the cpEGFP moiety inserted in green fluorescent genetically encoded Ca^{2+} indicators for optical imaging (G-GECO) (Zhao et al., 2011), GCaMP (Akerboom et al., 2012), GACH (Jing et al., 2018), and GRAB_{DA} (Sun et al., 2018) affects the fluorescence response of cpEGFP-based indicators. Thus, we systematically truncated the linker, which starts with the entire flexible ICL3 of α_2 AR surrounding cpEGFP (Figure 1B). We initially screened 275 linker-length variant proteins and identified a sensor (GRAB_{NE0.5m}) truncated at the S295 and R360 sites of α_2 AR with a modest response to NE (Figure 1B, right). From this prototype, we screened random mutations of seven amino acids close to the cpEGFP moiety: two (GG) on the N-terminal and five (GGAAA) on the C-terminal side of cpEGFP (Figure 1C). Among approximately 200 mutant candidates generated from GRAB_{NE0.5m}, we found GRAB_{NE1m}, which contains a glycine-to-threonine mutation at position C1, and exhibited the best performance with respect to $\Delta F/F_0$ and brightness (Figure 1C, middle and right). We hypothesize that GRAB_{NE}

(C) Optimizing the GRAB_{NE} sensors by mutational screening of the insertion linker. NE0.5m was used as a template, and the indicated amino acids on N-terminal and C-terminal sides of the cpEGFP insert were mutated individually. Sensor GRAB_{NE1m} (indicated by the pink squares) was identified due to having the strongest response ($\Delta F/F_0$) and brightness relative to the original NE0.5m sensor (indicated by the dashed line at 1.0).

(D) Tuning the sensor's affinity for NE by introducing mutations in the GPCR. Magnified views of the ligand-binding pocket from the cytosol are shown; key residues involved in ligand binding and inducing a conformational change upon ligand binding are indicated. The middle shows example images of HEK293T cells expressing the indicated GRAB_{NE} sensors; EGFP fluorescence is shown in the left column, and the fluorescence response in the presence of 100 μM NE is shown in the right column. Shown at the right are the normalized dose-response curves for the three GRAB_{NE} sensors, with EC₅₀ values (top) and the average fluorescence change in response to 100 μM NE (bottom); $n = 21$ –67 cells from 3–5 cultures for each sensor.

The scale bars in (A) and (D) represent 10 μm . Unless noted, values with error bars indicate mean \pm SEM. *** $p < 0.001$ (Student's *t* test). See also Figure S1.

shares a similar mechanism of fluorescence modulation as GCaMP sensors (Akerboom et al., 2009, 2012). Namely, ligand binding induces a conformational change of the binding protein (i.e., CaM in GCaMP), which alters the chemical environment, causing de-protonation of the cpEGFP chromophore and the resulting increase in fluorescence.

We expressed GRAB_{NE1m} in HEK293T cells and applied NE at different concentrations. NE induced a fluorescence change in GRAB_{NE1m}-expressing cells in a dose-dependent manner, with a half maximal effective concentration (EC₅₀) of 930 nM and a maximum $\Delta F/F_0$ of approximately 230% in response to a saturating concentration of NE (100 μ M; Figure 1D, middle and right). We also introduced mutations in α 2AR in order to increase its NE detection sensitivity. We found that a single T6.34K point mutation (Ren et al., 1993)—which is close to the highly conserved E6.30 site—resulted in a 10-fold increase in sensitivity (EC₅₀ \sim 83 nM) to NE compared with GRAB_{NE1m}. This sensor, which we call GRAB_{NE1h} (following the naming convention of GRAB_{DA}, “m” means medium and “h” means high affinity; Sun et al., 2018), had a maximum $\Delta F/F_0$ of \sim 130% in response to 100 μ M NE. As a control, we also generated GRAB_{NEmut}, which has the mutation S5.46A at the putative ligand-binding pocket and therefore is unable to bind NE (Figure 1D); this control sensor has similar brightness and membrane trafficking (Figures S1 and S2A) but does not respond to NE even at 100 μ M (Figure 1D, middle and right).

We examined whether our GRAB_{NE} sensors can capture the rapid dynamic properties of NE signaling, including its release, recycling, and degradation. We bathed GRAB_{NE1h}-expressing HEK293T cells in a solution containing 1-(2-nitrophenyl) ethoxy-carbonyl (NPEC)-caged NE. A focused spot of 405-nm light was applied to locally uncage NE by photolysis (Figure 2A). Transient photolysis induced a robust increase in fluorescence in GRAB_{NE1h}-expressing cells (mean on time constant 137 ms; single exponential fit), which was blocked by application of the α 2-adrenergic receptor antagonist yohimbine (Figures 2B and 2C). To characterize both the on and off rates (τ_{on} and τ_{off} , respectively) of the GRAB_{NE} sensors, we locally and subsequently applied NE and yohimbine to GRAB_{NE}-expressing cells using rapid perfusion and measured the fluorescence response using high-speed line scanning (Figures 2D and 2E). The average delay of the perfusion system itself (measured by fitting the fluorescence increase in the co-applied red fluorescent dye Alexa 568) was 34 ms (Figure 2F). Fitting the fluorescence change in each sensor with a single exponential function yielded an average τ_{on} of 72 and 36 ms for GRAB_{NE1m} and GRAB_{NE1h}, respectively, and an average τ_{off} of 680 and 1,890 ms for GRAB_{NE1m} and GRAB_{NE1h}, respectively (Figures 2E and 2F). The faster on rate and slower off rate of GRAB_{NE1h} compared to GRAB_{NE1m} are consistent with its relatively higher affinity for NE.

High ligand specificity is an essential requirement for tools designed to detect structurally similar monoamine-based molecules. Importantly, our GRAB_{NE} sensors, based on α 2AR, responded to both NE and epinephrine (Epi), but not other neurotransmitters around physiological concentrations (Figure 2G). The sensors also responded to the α 2AR agonist brimonidine, but not the β 2-adrenergic receptor agonist isoprenaline, indicating receptor-subtype specificity. Moreover, the NE-induced

fluorescence increase in GRAB_{NE}-expressing cells was blocked by the α -adrenergic receptor antagonist yohimbine, but not the β -adrenergic receptor antagonist ICI 118,551. Because NE and dopamine (DA) are structurally similar yet functionally distinct, we characterized how our GRAB_{NE} sensors respond to various concentrations of DA and NE. Wild-type α 2AR has an 85-fold higher affinity for NE versus DA (Figure 2H, right). Our GRABs bracketed this selectivity, with GRAB_{NE1m} at 350-fold higher affinity for NE, whereas GRAB_{NE1h} had a 37-fold higher affinity for NE (Figure 2H, left and middle). In contrast, FSCV was unable to differentiate between NE and DA, producing nearly identical responses to similar concentrations of NE and DA (Figures 2I and S2D; Robinson et al., 2003). To test photostability, we continuously illuminated GRAB_{NE}-expressing HEK293T cells using either 1-photon (confocal) or 2-photon laser microscopy and found that GRAB_{NE} sensors were more photostable than EGFP under both conditions (Figure S2C). Taken together, these data suggest that the GRAB_{NE} sensors can be used to measure the dynamic properties of noradrenergic activity with high specificity for NE over other neurotransmitters.

Next, we examined whether our GRAB_{NE} sensors trigger GPCR-mediated downstream signaling pathways. Bathing GRAB_{NE1m}-expressing cells in a saturating concentration of NE for 2 h resulted in no internalization of GRAB_{NE1m} (Figure 2J). Consistent with this, both GRAB_{NE1m} and GRAB_{NE1h} induced little β -arrestin-mediated signaling in a TANGO assay, even at the highest concentration of NE tested (Figure 2K), suggesting no coupling to β -arrestin signaling. In addition, GRAB_{NE1m} and GRAB_{NE1h} had drastically reduced downstream Gi coupling compared to wild-type α 2AR, which was measured using a Gi-coupling-dependent luciferase complementation assay (Figure 2L; Wan et al., 2018). We also found that G protein activation by GRAB_{NE1m} measured by the highly sensitive transforming growth factor α (TGF- α) shedding assay was reduced by about 100-fold compared to the wild-type receptor α 2AR (Figure S2B; Inoue et al., 2012). Finally, blocking G protein activation by treating cells with pertussis toxin (Figure 2M) had no effect on the fluorescence response of either GRAB_{NE1m} or GRAB_{NE1h}, indicating that the fluorescence response of GRAB_{NE} sensors did not require G protein coupling (Rasmussen et al., 2011a). Taken together, these data indicate that GRAB_{NE} sensors can be used to report NE dynamics without inadvertently engaging GPCR downstream signaling.

Characterization of GRAB_{NE} Sensors in Cultured Neurons

The expression, trafficking, and response of proteins can differ considerably between neurons and cell lines (Marvin et al., 2013; Zou et al., 2014). To characterize the performance of GRAB_{NE} sensors in neurons, we co-expressed GRAB_{NE} together with several neuronal markers in cultured cortical neurons. Both GRAB_{NE1m} and GRAB_{NEmut} trafficked to the cell membrane and colocalized with the membrane-targeted marker RFP-CAAX (Figures 3A and 3B). Upon bath application of a saturating concentration of NE, GRAB_{NE1m} and GRAB_{NE1h} had a peak $\Delta F/F_0$ of approximately 230% and 150%, respectively, whereas GRAB_{NEmut} had no response (Figures 3D and 3E), similar to our results obtained with HEK293T cells. Moreover, the NE-induced

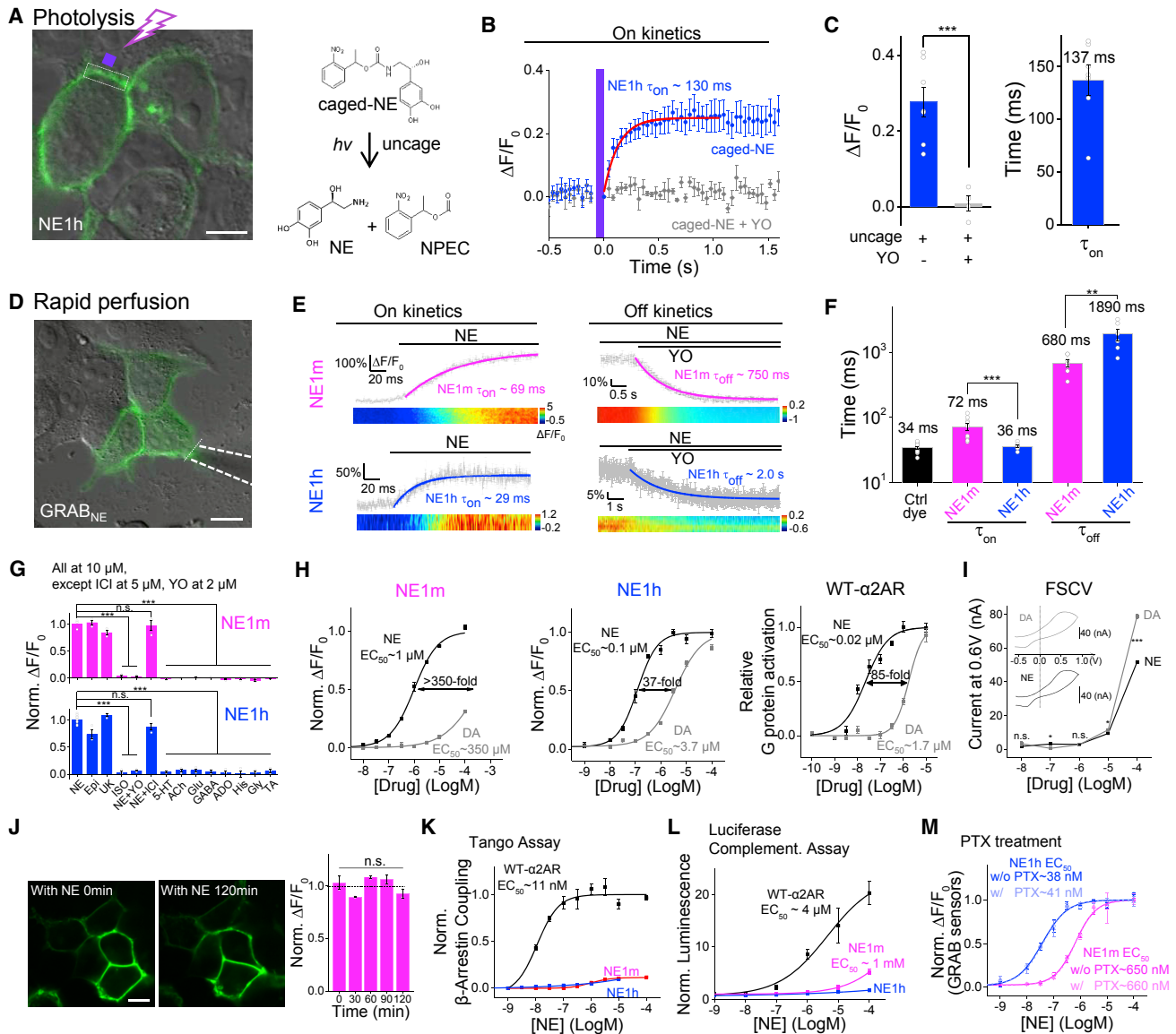


Figure 2. Characterization of GRAB_{NE} Sensors in Cultured Cells

(A–C) HEK293T cells were loaded with NPEC-NE, which was uncaged by photolysis with a pulse of 405-nm light (A). Uncaging caused a rapid increase in GRAB_{NE1h} fluorescence, which was blocked in the presence of 10 μ M yohimbine (YO). The data in (B) represent 3 trials each, and the data in (C) represent 7 cells from 3 cultures. The white dotted square indicates the image region, and the purple square indicates the illumination region.

(D–F) NE was applied to HEK293T cells (D) expressing GRAB_{NE1m} or GRAB_{NE1h} to measure τ_{on} . Yohimbine (YO) was then applied in order to measure τ_{off} ; representative traces (E) and quantification data (F) are shown; the white dotted line indicates the line-scanning region. $n \geq 6$ cells from 6 cultures.

(G) The indicated compounds were applied to GRAB_{NE1m} and GRAB_{NE1h}, and the change in fluorescence relative to NE is plotted.

(H) Dose-response curves for GRAB_{NE1m}, GRAB_{NE1h}, and wild-type α 2AR for NE and DA, with EC₅₀ values shown; $n \geq 3$ wells with 100–300 cells each.

(I) Fast-scan cyclic voltammetry measurements in response to increasing concentrations of NE and DA. The insets show exemplar cyclic voltammograms of NE and DA at 100 μ M, with peak current occurring at \sim 0.6 V.

(J) Time course of $\Delta F/F_0$ for GRAB_{NE} sensors measured over a 2-h time frame; note that the fluorescent signal remained at the cell surface even after 180 min, indicating no measurable internalization or desensitization. $n = 2$ wells with 100–300 cells each.

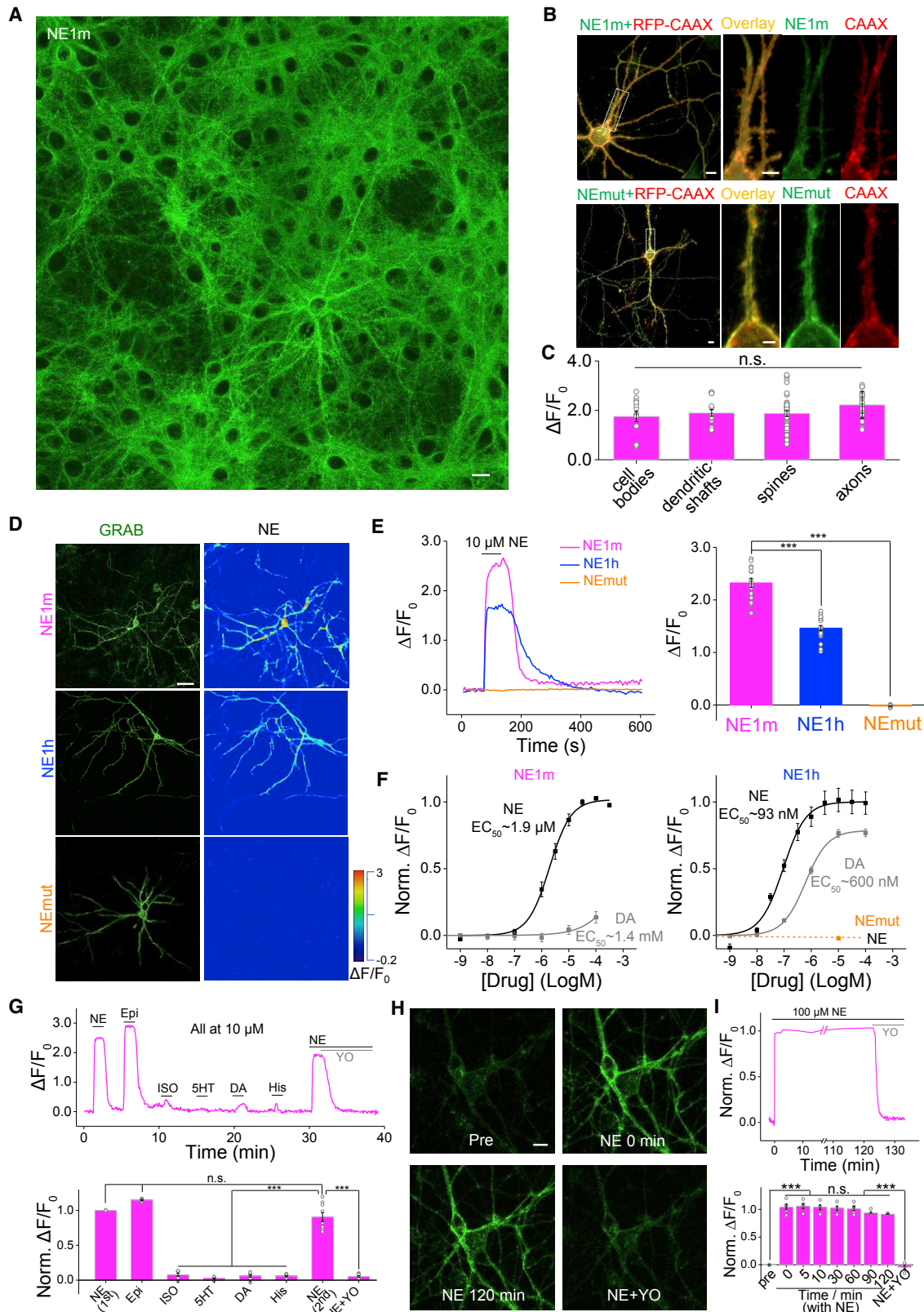
(K) A TANGO assay was performed in order to measure β -arrestin-mediated signaling by GRAB_{NE1m}, GRAB_{NE1h}, and wild-type α 2AR in the presence of increasing concentrations of NE; $n = 4$ wells with $\geq 10^5$ cells each.

(L and M) GRAB_{NE} sensors do not couple to downstream G protein signaling pathways.

(L) Wild-type α 2AR, but not GRAB_{NE1m} or GRAB_{NE1h}, drives G α_i signaling measured using a luciferase complementation assay; $n = 3$ wells with $\geq 10^5$ cells each.

(M) Disrupting of G protein activation with pertussis toxin (PTX) does not affect the NE-induced fluorescence change in GRAB_{NE1m} or GRAB_{NE1h}. $n = 3$ wells with ≥ 100 –300 cells each.

The scale bars in (A), (D), and (J) represent 10 μ m. * $p < 0.05$, ** $p < 0.01$, and *** $p < 0.001$; n.s., not significant (Student's *t* test). See also Figure S2.



(legend on next page)

responses in GRAB_{NE1m}-expressing cells were similar among various subcellular compartments identified by co-expressing GRAB_{NE1m} with either the axonal marker synaptophysin (SYP) or the dendritic marker PSD95, suggesting that GRAB_{NE} sensors enabled the detection of NE throughout the neurons (Figure 3C). Both GRAB_{NE1m}- and GRAB_{NE1h}-expressing neurons had a dose-dependent fluorescence increase in response to NE, with mean EC₅₀ values of 1.9 μ M and 93 nM, respectively (Figure 3F). Consistent with high selectivity for NE, GRAB_{NE1m} and GRAB_{NE1h} had a 1,000-fold and 7-fold higher affinity, respectively, for NE versus DA (Figure 3F). Moreover, GRAB_{NE1m} responded specifically to NE and Epi, but not to several other neurotransmitters and ligands, including isoprenaline, histamine, dopamine, and serotonin (Figure 3G). Similar to our results in HEK293T cells, inhibiting G protein activation with pertussis toxin did not affect the NE-induced fluorescence change in GRAB_{NE1m} in cultured neurons (Figure S2E), suggesting G protein coupling was not involved in the fluorescence change of GRAB_{NE1m}. Finally, bathing GRAB_{NE1m}-expressing neurons in 100 μ M NE for 2 h did not cause detectable internalization of the sensor. The fluorescence increase was stable for the entire period and blocked completely by yohimbine (Figures 3H and 3I). Thus, our GRAB_{NE} sensors have the necessary affinity and specificity to faithfully measure noradrenergic signaling in neurons.

Characterization of GRAB_{NE} Sensors in Both Cultured and Acute Brain Slices

To further test the performance of GRAB_{NE} sensors *in vitro*, we expressed GRAB_{NE1m} and GRAB_{NE1h} in cultured hippocampal slices using a Sindbis virus expression system (Figure S3A). In both GRAB_{NE1m}- and GRAB_{NE1h}-expressing CA1 neurons, exogenous application of NE in artificial cerebrospinal fluid (ACSF)—but not ACSF alone—evoked a robust increase in fluorescence (Figures S3B–S3D). In contrast, NE had no detectable effect on GRAB_{NEmut}-expressing neurons (Figures S3C and S3D). Application of several α -adrenergic receptor agonists, including epinephrine and brimonidine, also generated fluorescence increases in GRAB_{NE1m}-expressing neurons (Figures S3C and S3F), consistent with data in cultured cells. The rise and decay kinetics of the change in fluorescence were second order, which reflects the integration of the time required to puff the drugs onto the cells and the sensor's response kinetics (Figures S3E and S3G). To test whether overexpression of NE sensors may affect endogenous NE receptors, we made simultaneous dual patch-clamp recordings and fluorescence imaging

from pairs of neighboring GRAB_{NE1m}-expressing and control non-expressing CA1 neurons (Figure S3H). Brief 10-ms NE puff applications evoked a large outward current in GRAB_{NE1m}-expressing and non-expressing neurons, as well as a concurrent fluorescence signal in GRAB_{NE1m}-expressing neurons, but not in control non-expressing neurons (Figures S3I–S3L). The NE receptor-mediated outward currents had the same amplitude, latency, signal-to-noise ratio, desensitization, rise time, and decay time constant in GRAB_{NE1m}-expressing and control non-expressing neurons (Figures S3I–S3L and S3M–S3O), suggesting no effect of overexpression of GRAB_{NE1m} on endogenous NE receptor function. Notably, GRAB_{NE1m} detected faster NE signals prior to the electrophysiologically recorded NE-activated outward currents.

We also prepared acute hippocampal slices in which GRAB_{NE1h} was expressed using an adeno-associated virus (AAV); in this acute slice preparation, GRAB_{NE1h}-expressing hippocampal neurons are innervated by noradrenergic fibers, which was confirmed by post hoc staining using an antibody against dopamine beta hydroxylase (Figures S4A and S4B). Application of electrical stimuli at 20 Hz for 1 s elicited a robust increase in GRAB_{NE1h} fluorescence, and this increase was blocked by the application of yohimbine (Figure S4C). Consistent with our results obtained using cultured slices, exogenous application of various α -adrenergic receptor agonists, including NE, Epi, and brimonidine—but not the β -adrenergic receptor agonist isoprenaline—evoked a fluorescence increase in GRAB_{NE1h}-expressing neurons, and this response was blocked by yohimbine, but not by the β -adrenergic receptor antagonist ICI 118,551 (Figure S4D). To examine whether expression of GRAB_{NE} sensors would alter neurons' physiology, we also compared the calcium signals between GRAB_{NE1h}-expressing neurons and control non-expressing neurons in acute hippocampus slices (Figures S4E–S4I). Overexpression of a high-affinity version of GRAB_{NE} sensor (GRAB_{NE1h}) did not alter the high potassium-induced calcium signals (Figures S4G–S4I), indicating no apparent perturbation on the excitability of neurons when overexpressing GRAB_{NE}.

We examined whether our GRAB_{NE} sensors can be used to monitor the dynamics of endogenous NE. We expressed GRAB_{NE1m} in the locus coeruleus (LC) (Figure 4A), which contains the majority of adrenergic neurons within the brain, and activation of LC neurons by salient stimuli, including physiological stress, looming, and electrical stimulation, concomitantly releases NE throughout many brain regions (Berridge and Waterhouse, 2003; Dugast et al., 2002; Schwarz and Luo, 2015).

Figure 3. Characterization of GRAB_{NE} Sensors in Cultured Neurons

(A–C) GRAB_{NE1m} is expressed in various plasma membrane compartments of cultured neurons (A). Cultured cortical neurons were co-transfected with GRAB_{NE1m} and RFP-CAAX to label the plasma membrane (B), and the fluorescence response induced by bath application of NE was measured in the cell body, dendritic shaft and spine, and axon (C). $n > 10$ neurons from 4 cultures.

(D and E) Cultured cortical neurons expressing GRAB_{NE1m} and GRAB_{NE1h}, but not GRAB_{NEmut}, respond to application of NE (10 μ M). EGFP fluorescence and pseudocolor images depicting the response to NE are shown in (D), and the time course and summary of peak $\Delta F/F_0$ are shown in (E). $n > 15$ neurons from 3 cultures.

(F) Dose-response curve for GRAB_{NE} sensors expressed in cultured cortical neurons in response to NE and DA. $n > 10$ neurons from 3 cultures.

(G) Example trace (top) and summary (bottom) of cultured neurons transfected with GRAB_{NE1m} and treated with the indicated compounds at 10 μ M each. $n = 9$ neurons from 3 cultures.

(H and I) The fluorescence change in GRAB_{NE1m} induced by 100 μ M NE is stable for up to 2 h. Representative images taken at the indicated times are shown in (H). An example trace and summary data are shown in (I). Where indicated, 10 μ M YO was added. $n = 5$ neurons from 3 cultures. The scale bars in (A), (B), and (H) represent 10 μ m; the scale bar in (D) represents 25 μ m. *** $p < 0.001$ (Student's *t* test). See also Figure S2.

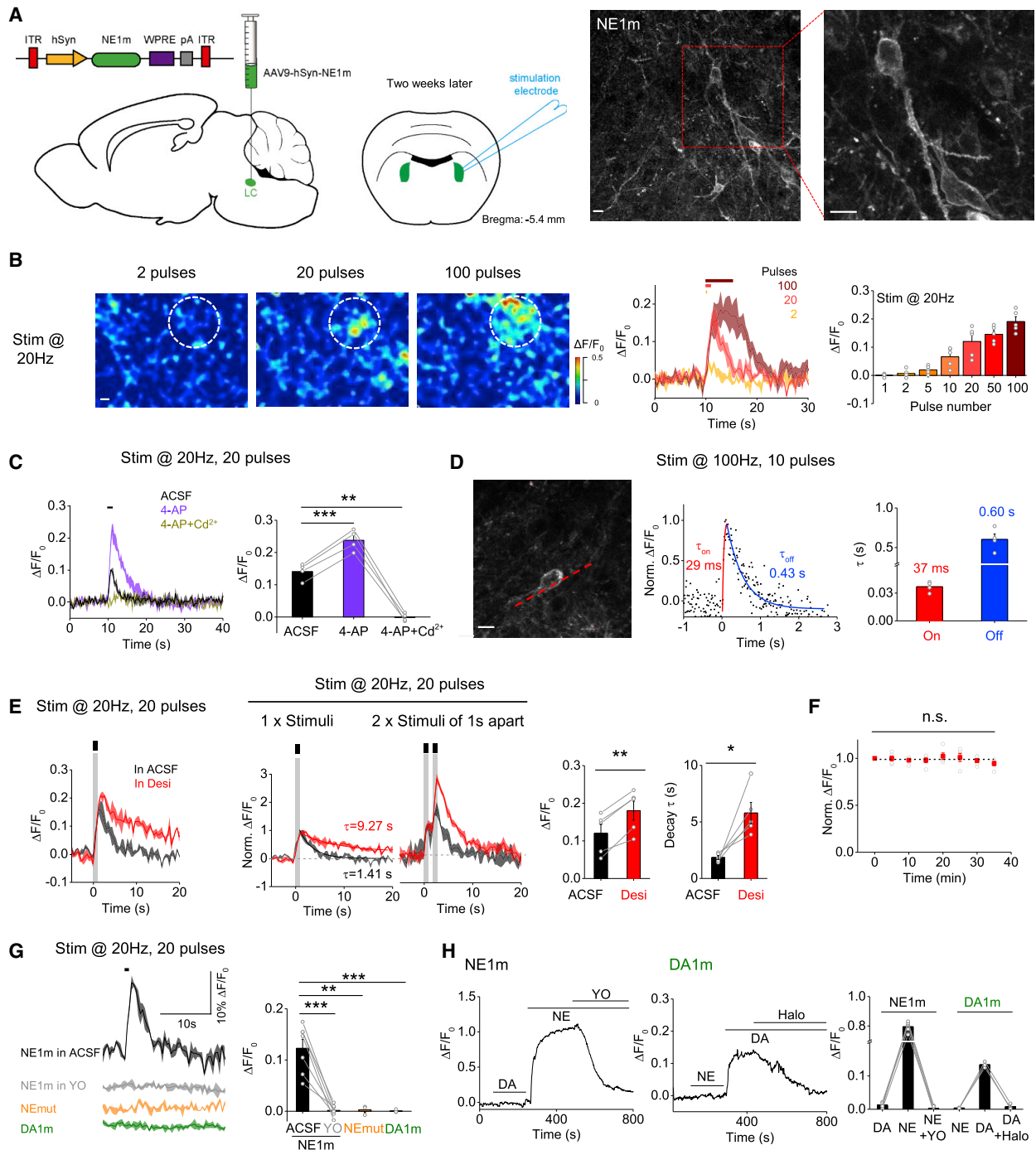


Figure 4. Release of Endogenous NE Measured in Mouse Brain Slices

(A) Left: schematic illustration of the slice experiments. An AAV expressing hSyn-GRAB_{NE1m} was injected into the LC; 2 weeks later, acute brain slices were prepared and used for electric stimulation experiments. Right: exemplar 2-photon microscopy images show the distribution of GRAB_{NE1m} in the plasma membrane of LC neurons.

(B) Left and middle: representative pseudocolor images and corresponding fluorescence changes in GRAB_{NE1m}-expressing neurons in response to 2, 20, and 100 pulses delivered at 20 Hz. The region of interest (ROI) (50- μ m diameter) for data analysis is indicated in the images. Right: summary of the peak fluorescence change in slices stimulated as indicated is shown; n = 5 slices from 5 mice.

(C) Exemplar traces and summary data of GRAB_{NE1m}-expressing neurons in response to 20 electrical stimuli delivered at 20 Hz in ACSF, 4-AP (100 μ M), or 4-AP with Cd²⁺ (100 μ M); n = 4 slices from 4 mice.

(legend continued on next page)

2 weeks after AAV injection, we prepared acute brain slices and observed GRAB_{NE1m} expression in the membrane of LC neurons using two-photon microscopy (Figure 4A). We then used electrical stimuli at 20 Hz to evoke the release of endogenous NE in the LC in the acute slices. Increasing the number of stimuli caused progressively stronger responses (Figure 4B). To estimate the concentration of NE after electrical stimulation, we also perfused the same slices with different concentrations of exogenous NE. Based on the calibration curve, we estimated that the volume-averaged NE concentration (NE_{Vol}) was $0.17 \pm 0.04 \mu\text{M}$ and $0.56 \pm 0.13 \mu\text{M}$ when stimulated with 2 or 20 pulses at 20 Hz, respectively (Figures S4J–S4M). Application of the voltage-activated potassium channel blocker 4-aminopyridine, which increases Ca²⁺ influx during action potentials, significantly increased the fluorescence response, whereas application of Cd²⁺ to block calcium channels abolished the stimulation-induced fluorescence increase (Figure 4C), consistent with presynaptic NE release being mediated by Ca²⁺ influx. We also performed line-scanning experiments in order to track the kinetics of endogenous NE release (Figure 4D, left). A brief electrical stimulation induced a rapid fluorescence response with a mean τ_{on} and τ_{off} of 37 ms and 600 ms, respectively (Figure 4D, middle and right). Taken together, these data indicate that GRAB_{NE1m} can be used to monitor the release of endogenous NE in real time.

NE released into the synaptic cleft is recycled back into the presynaptic terminal by the norepinephrine transporter (NET). We therefore tested the sensitivity of GRAB_{NE1m} to NET blockade using desipramine in acute brain slices. In the presence of desipramine, electrical stimuli caused larger fluorescence responses in GRAB_{NE1m}-expressing neurons compared with ACSF alone (Figure 4E). Moreover, desipramine significantly slowed down the decay kinetics of fluorescence signals, consistent with reduced reuptake of extracellular NE into the presynaptic terminal. To rule out the possibility that the change in the fluorescence response was caused by synaptic modulation over time, we applied repetitive electrical stimuli at 5-min intervals to GRAB_{NE1m}-expressing neurons and found that the stimulation-evoked response was stable for at least 40 min (Figure 4F). Finally, we examined the specificity of the stimulation-induced response. Compared with a robust response in control conditions, the α -adrenergic antagonist yohimbine blocked the response; moreover, no response was elicited in LC neurons expressing GRAB_{NEmut} or in LC neurons expressing a dopamine sensor (GRAB_{DA1m}; Figure 4G). In contrast, cells expressing GRAB_{DA1m} responded robustly to the applica-

tion of DA, and the GRAB_{NE1m} and GRAB_{DA1m} responses were abolished by yohimbine or the dopamine receptor antagonist haloperidol, respectively (Figure 4H). Taken together, these data indicate that GRAB_{NE} sensors are both sensitive and specific for detecting endogenous noradrenergic activity in LC neurons.

GRAB_{NE} Sensors Detect Both Exogenous NE Application and Endogenous NE Release in Awake Zebrafish

Zebrafish is a genetically accessible vertebrate species and optically transparent during development, thus serving as a suitable model for *in vivo* imaging. We generated the transgenic zebrafish line Tg(HuC:GRAB_{NE1m}), which pan-neuronally expressed the GRAB_{NE1m} sensor. Pan-neuronal expression was confirmed by GRAB_{NE1m} basal fluorescence on the cell membrane of neurons throughout the brain (Figure 5A). Bath application of 50 μM NE—but not DA at the same concentration—elicited a robust increase in fluorescence intensity that was blocked completely by the subsequent application of 50 μM yohimbine (Figures 5B–5D). In addition, a separate zebrafish line expressing GRAB_{NEmut} did not respond to NE (Figures 5C and 5D).

Next, we investigated whether GRAB_{NE1m} can be used to measure the dynamics of endogenous noradrenergic activity induced by a salient stimulus. Visual looming triggers a robust escape response in zebrafish (Berridge and Waterhouse, 2003; Li et al., 2018). We applied repeated looming stimuli during confocal imaging to record the fluorescence of GRAB_{NE1m}-expressing neurites in the optic tectum (Figure 5E). Each looming stimulus induced a time-locked increase in GRAB_{NE1m} fluorescence, which was blocked by bath application of yohimbine but unaffected by the β -adrenergic receptor antagonist ICI 118,551 (Figures 5F and 5G). Similarly, looming stimuli induced a time-locked, repeatable fluorescence increase in GRAB_{NE1h} transgenic zebrafish (Figures S5A and S5B). In contrast, the same looming stimuli had no effect in zebrafish expressing GRAB_{NEmut} (Figures 5F and 5G). In addition, adding the NE reuptake inhibitor desipramine slowed the decay of the fluorescence signal (Figure 5H). By sparsely expressing GRAB_{NE1m} in individual neurons in zebrafish larvae via transient transfection, we were also able to record robust signals at single-cell resolution in response to repetitive looming stimuli (Figures 5I–5K), confirming that our GRAB_{NE} sensors can be used to sense NE release at the single-cell level with high spatiotemporal resolution. Finally, by expressing jRGECO1a, we compared both spontaneous and looming-evoked calcium activities in the optic tectum between

(D) Kinetic properties of the electrically evoked fluorescence responses in GRAB_{NE1m}-expressing LC neurons. Left image shows a GRAB_{NE1m}-expressing LC neuron for line scan analysis (red dashed line). (Middle and right) An exemplar trace and summary of the responses elicited in GRAB_{NE1m}-expressing neurons before and after 10 pulses delivered at 100 Hz are shown; $n = 4$ slices from 4 mice.

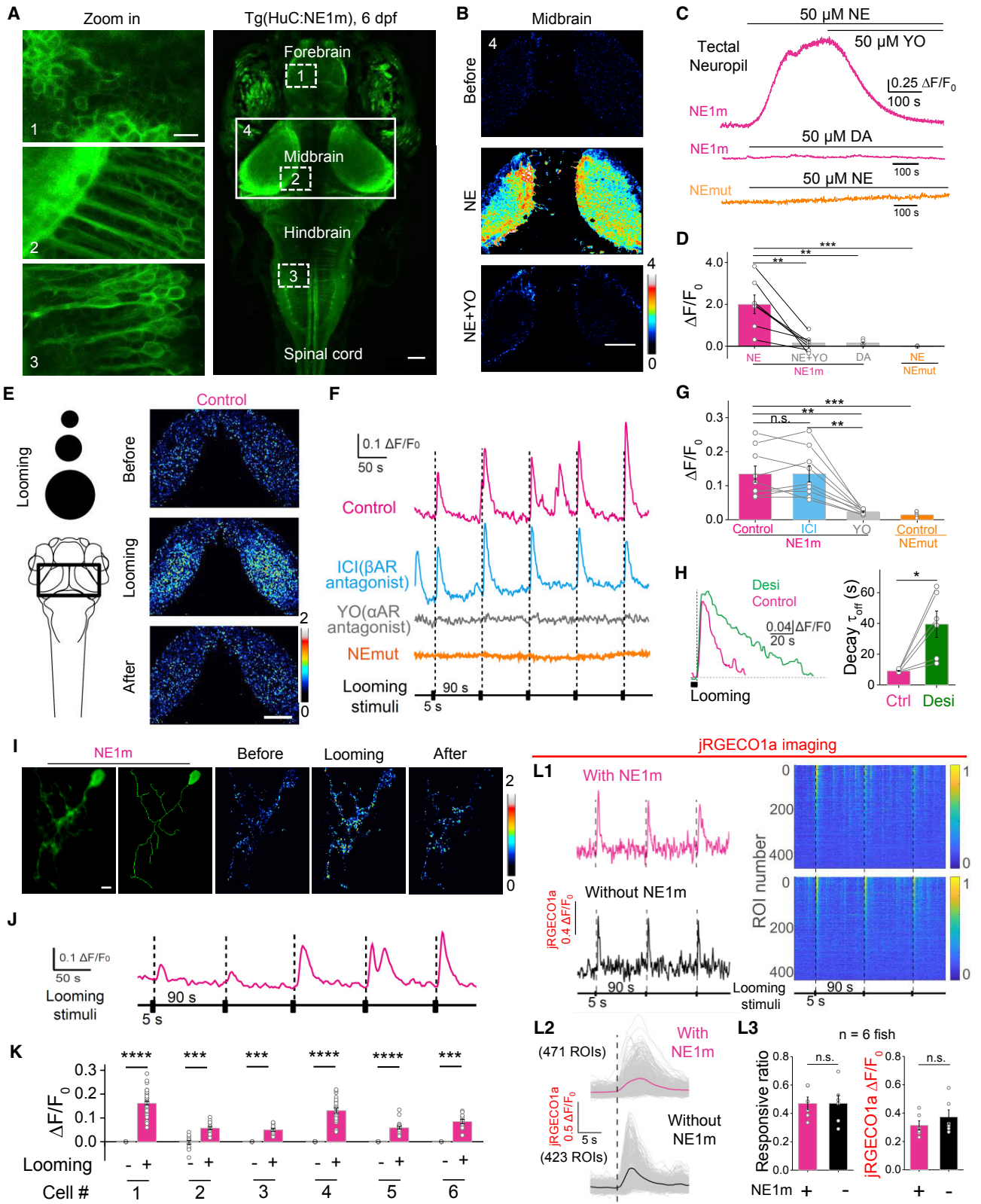
(E) The norepinephrine transporter blocker desipramine (Desi, 10 μM ; red) increases the effect of electrical stimuli (20 pulses at 20 Hz) or two trains of stimuli with a 1-s interval compared to ACSF (black traces). $n = 5$ slices from 5 mice.

(F) The fluorescence response in GRAB_{NE1m}-expressing neurons is stable. Eight stimuli (20 pulses at 20 Hz) were applied at 5-min intervals, and the response (normalized to the first train) is plotted against time. $n = 5$ slices from 5 mice.

(G) Traces and summary data of the fluorescence response measured in neurons expressing GRAB_{NE1m} (the same plot in E, left, gray curve), GRAB_{NEmut}, or GRAB_{DA1m} in response to 20 pulses delivered at 20 Hz in the presence of ACSF or 20 μM YO; $n = 3$ –7 slices from 3–7 mice.

(H) Traces and summary data of the fluorescence response measured in neurons expressing GRAB_{NE1m} or GRAB_{DA1m}. Where indicated, 50 μM NE, 50 μM DA, 20 μM YO, and/or 20 μM haloperidol (Halo) was applied to the cells. $n = 3$ –5 slices from 3–5 mice.

The scale bars represent 10 μm . * $p < 0.05$, ** $p < 0.01$, and *** $p < 0.001$ (Student's *t* test). See also Figure S4.



(legend on next page)

zebrafish with or without GRAB_{NE1m} expression and observed no significant difference in activity (Figures S5C1–S5C3 and 5L), suggesting no adverse effects when expressing GRAB_{NE} sensors *in vivo*. Taken together, these data indicate that GRAB_{NE} sensors are sensitive and specific for detecting *in vivo* NE release in a common model system.

GRAB_{NE1m} Detects Optogenetically Evoked NE Release in Freely Moving Mice

Having demonstrated proof of concept in a relatively simple *in vivo* vertebrate system, we next examined whether the GRAB_{NE} sensors can be used to monitor noradrenergic activity in the mammalian brain. We virally expressed GRAB_{NE1m} (non-Cre dependent) together with the optogenetic actuator C1V1 (Cre-dependent) in the LC of Th-Cre mice (Figure 6A). Optogenetic stimulation of LC noradrenergic neurons using 561-nm laser pulses reliably evoked an increase in GRAB_{NE1m} fluorescence in fiber photometry recording of freely moving mice. Moreover, intraperitoneal (i.p.) injection of desipramine produced a slow progressive increase in basal GRAB_{NE1m} fluorescence (consistent with an increase in extracellular NE levels) and caused an increase in the magnitude and decay time of the light-activated responses. Intraperitoneal (i.p.) injection of yohimbine abolished both the increase in basal GRAB_{NE1m} fluorescence and the light-evoked responses (Figures 6B–6D). In contrast, treating mice with either GBR 12909 (a selective blocker of dopamine transporters) or eticlopride (a specific D2R antagonist) had no effect on the light-evoked responses in GRAB_{NE1m} fluorescence (Figures 6C–6E). To further test the selectivity of GRAB_{NE1m} between NE and DA, we co-expressed GRAB_{NE1m} and DIO-C1V1 both in the LC and in the substantia nigra pars compacta (SNc) of Th-Cre mice (Figure 6F). In these mice, optogenetic stimulation of dopaminergic neurons in the SNc did not cause any changes in the GRAB_{NE1m} fluorescence in the SNc. In contrast, stimulating NE neurons in the LC produced a robust increase in GRAB_{NE1m} fluorescence (Figures 6F and 6G). These results confirmed that the increase of GRAB_{NE1m} fluorescence reflects the release of endogenous NE from noradrenergic neurons in the LC.

Using GRAB_{NE1m} to Track Endogenous NE Dynamics in the Mouse Hypothalamus during Freely Moving Behaviors

In the brain, the hypothalamus mediates a variety of innate behaviors essential for survival, including feeding, aggression, mating, parenting, and defense (Hashikawa et al., 2016; Sokolowski and Corbin, 2012; Yang and Shah, 2016). The hypothalamus receives extensive noradrenergic projections (Moore and Bloom, 1979; Schwarz and Luo, 2015; Schwarz et al., 2015) and expresses an abundance of α 2-adrenergic receptors (Leibowitz, 1970; Leibowitz et al., 1982). Microdialysis studies found that the hypothalamus is among the brain regions that release the high levels of NE during stress (Mc Quade and Stanford, 2000; Pacak et al., 1995; Shekhar et al., 2002; Tanaka, 1999). To better understand NE dynamics in the hypothalamus under stress, we virally expressed hSyn-GRAB_{NE1m} in the lateral hypothalamus of C57BL/6 mice. 3 weeks after virus injection, we performed fiber photometry recordings of GRAB_{NE1m} fluorescence during a variety of stressful and non-stressful behaviors in freely moving mice (Figure 7).

During forced swimming and tail suspension tests, both of which were stressful, we observed a significant increase in GRAB_{NE1m} fluorescence. During forced swimming, the fluorescence signal increased continuously, regardless of the animal's movements and started to decrease only after the animal was removed from the water (Figures 7C1, 7D1, and 7E1). During the 60-s tail suspension test, the signal began to rise when the animal was first pursued by the experimenter's hand, increased continuously while the animal was suspended by the tail, and decreased rapidly back to baseline after the animal was returned to the ground (Figures 7C2, 7D2, and 7E2). Additionally, when a human hand was placed in front of the animal, we observed a small and transient increase in GRAB_{NE1m} fluorescence (Figures 7C3, 7D3, and 7E3). In contrast, when a conspecific intruder of either the same or the opposite sex was introduced into the test animal's cage, we observed no change or a decrease in GRAB_{NE1m} signals both during the initial introduction and subsequent social interactions, including social approach, being sniffed, or sniffing (Figures 7C4, 7D4, and 7E4 and 7C5, 7D5, and

Figure 5. GRAB_{NE} Can Be Used to Measure Noradrenergic Activity *In Vivo* in Transgenic Zebrafish

(A) *In vivo* confocal image of a Tg(HuC:GRAB_{NE1m}) zebrafish expressing GRAB_{NE1m} in neurons driven by the HuC promoter. Larvae at 6 days post-fertilization were used.

(B–D) Bath application of NE (50 μ M), but not DA (50 μ M), elicits a significant increase in fluorescence in the tectal neuropil of Tg(HuC:GRAB_{NE1m}) zebrafish, but not in GRAB_{NEmut} zebrafish, and this increase is blocked by YO (50 μ M), but not ICI 118,551 (50 μ M). Pseudocolor images (B), raw traces (C), and statistical results (D) are shown. $n = 7$.

(E–H) Visual looming stimuli evoke the release of endogenous NE in the midbrain of GRAB_{NE1m} zebrafish, but not in GRAB_{NEmut} zebrafish. The looming stimuli paradigm is shown in the left of (E). Raw traces (F) and statistical results (G) are shown. Where indicated, YO (50 μ M) or ICI 118,551 (50 μ M) was applied. Desipramine (Desi, 50 μ M) application slowed the decay of looming-induced NE release (H). $n = 6$ for GRAB_{NEmut} and $n = 9$ for the others.

(I–K) Single-cell labeling of GRAB_{NE1m} in the midbrain of zebrafish larva (I), with looming-evoked responses shown in (I) and (J). The summary data for 6 labeled cells are shown in (K).

(L) Looming-evoked calcium responses of optic tectal neurons reported by jRGECO1a show no difference with or without HuC:GRAB_{NE1m} overexpression. Exemplar traces of looming-evoked responses of single tectal neurons are shown (L1, left). Responsive neurons sorted as descending amplitudes are shown (L1, right). 20 s before each stimulus as the baseline is shown. Averaged looming-evoked jRGECO1a responses of every neuron (L2, gray lines) and the averaged responses of all neurons (L2, red line and black line, respectively) are shown. The responsive ratio and averaged amplitude of every fish are shown in (L2). $n = 6$.

The scale bar shown in (A, left) represents 10 μ m; the scale bars shown in (A, right), (B), and (E) represent 50 μ m. The scale bar shown in (I) represents 5 μ m. * $p < 0.05$, ** $p < 0.01$, *** $p < 0.001$, and **** $p < 0.0001$ (Wilcoxon matched-pairs signed rank test in H; all others were analyzed using the paired or unpaired Student's *t* test). See also Figure S5.

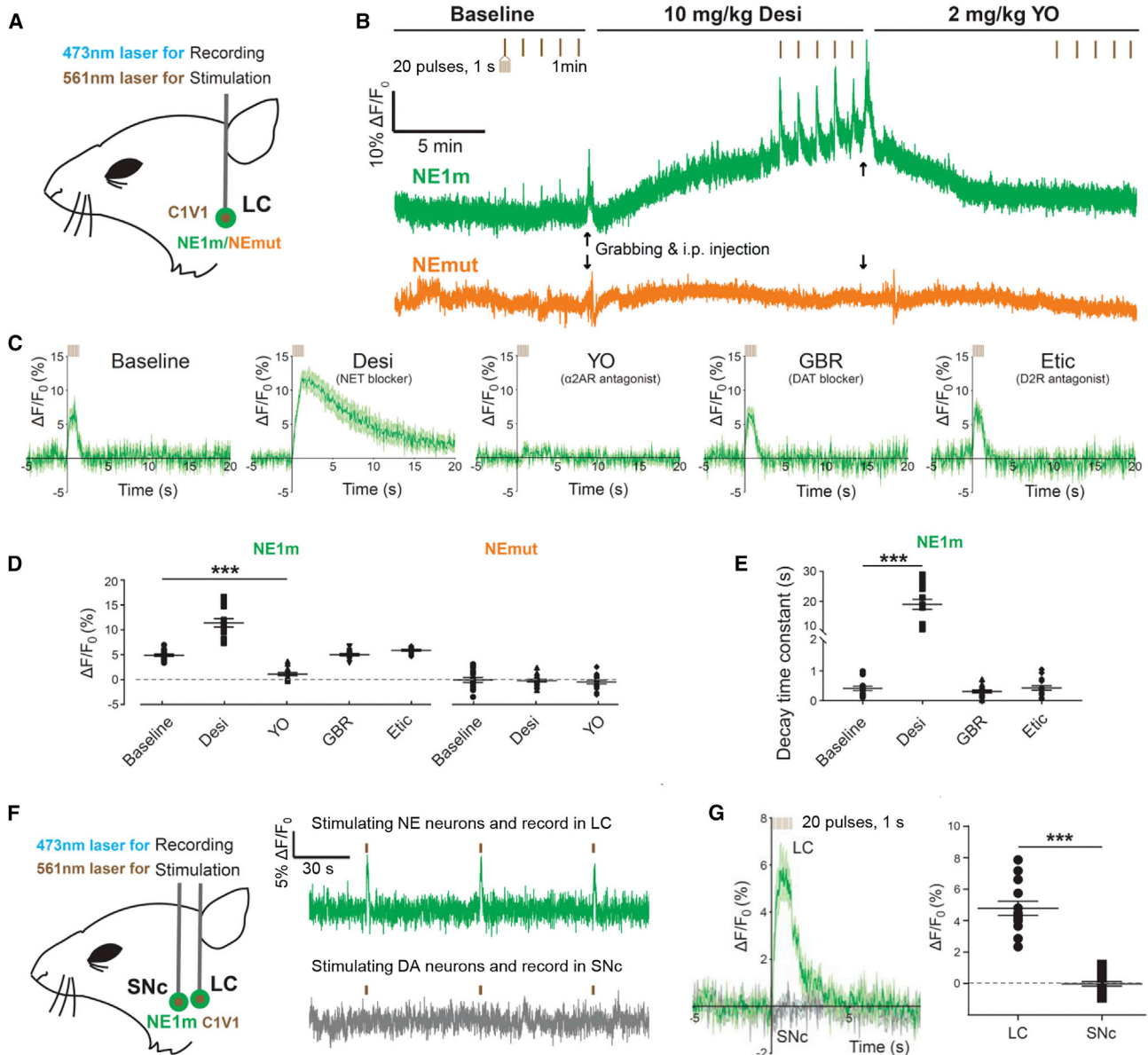


Figure 6. GRAB_{NE1m} Can Be Used to Measure Optogenetically Stimulated Noradrenergic Activity *In Vivo* in Freely Moving Mice

(A) Schematic illustration depicting the experimental design for recording GRAB_{NE1m} and GRAB_{NEmut} fluorescence in response to optical stimulation of C1V1 in the locus coeruleus (LC).

(B) Representative traces of optogenetically stimulated GRAB_{NE1m} (top) and GRAB_{NEmut} (bottom) activity in the LC before (baseline, left), 15 min after an i.p. injection of the NET blocker desipramine (10 mg/kg, middle), and 15 min after an i.p. injection of the α 2AR antagonist yohimbine (2 mg/kg, right). The vertical tick marks indicate the optogenetic stimuli. Black arrows represent the timing for grabbing and i.p. injection.

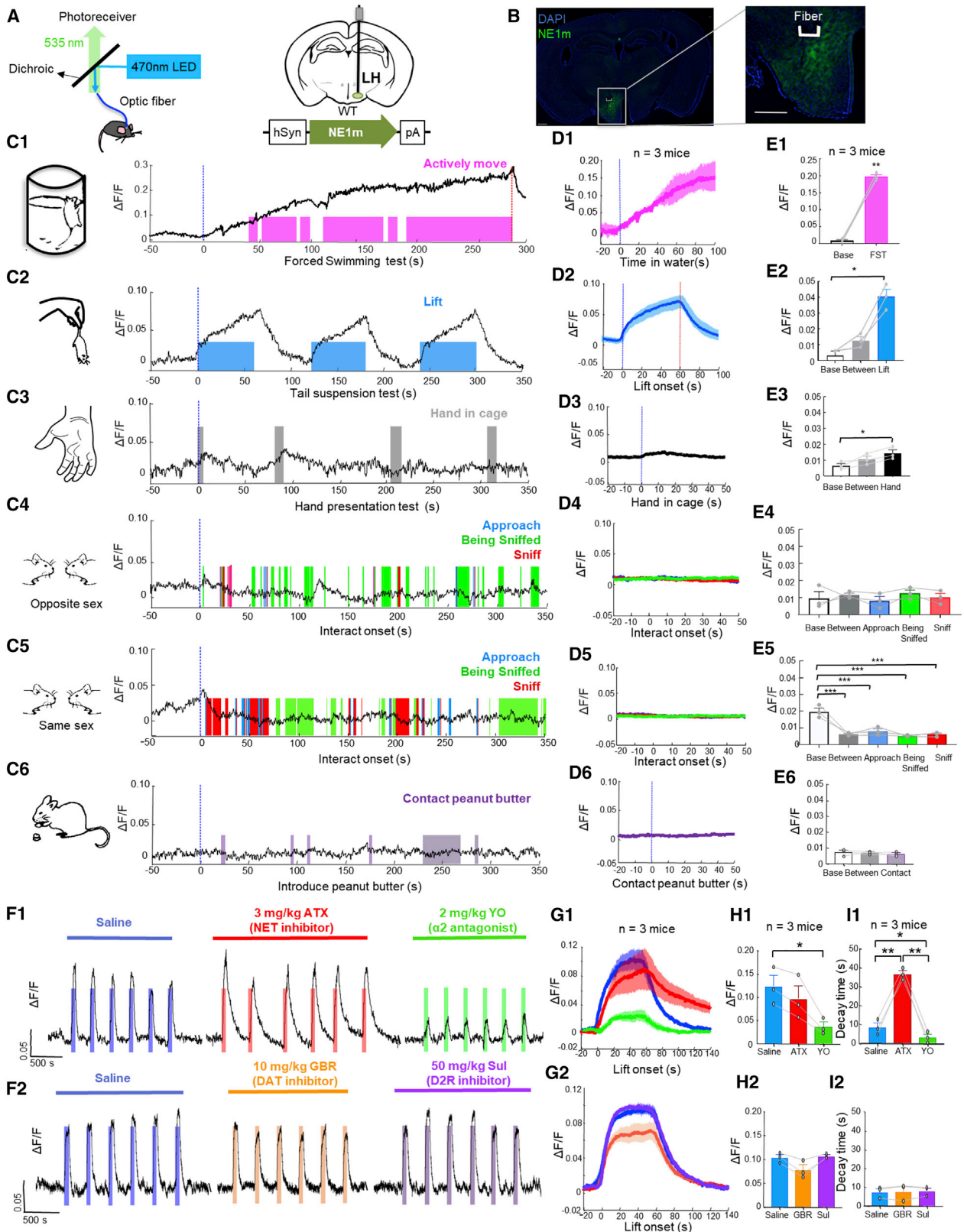
(C–E) Average traces of GRAB_{NE1m} fluorescence (C), summary data (D), and the decay time constant (E) in response to optical stimulation in the LC following treatment with the indicated compounds. $n = 15$ trials from 3 mice for each condition.

(F and G) Schematic illustration (F, left), representative traces (F, right), average fluorescence change (G, left), and summary data (G, right) for GRAB_{NE1m} in response to optical stimulation of noradrenergic neurons in the LC and dopaminergic neurons in the SNc.

*** $p < 0.001$ (for D and E, one-way ANOVA; for G, Student's *t* test).

7E5). Similarly, sniffing or eating palatable food (i.e., peanut butter) did not evoke detectable GRAB_{NE1m} fluorescence signals (Figures 7C6, 7D6, and 7E6). In control animals that expressed GRAB_{NEmut} in the lateral hypothalamus, we observed no increase in fluorescence during all examined behavioral tests,

including the forced swimming test and the tail suspension test, suggesting that movement artifacts contribute minimally to the detected signal change (Figure S6). These data altogether provide evidence indicating that noradrenergic activity in the lateral hypothalamus occurs primarily under stressful conditions.



(legend on next page)

Finally, to confirm the specificity of the GRAB_{NE1m} sensor for monitoring NE dynamics over other monoamine neurotransmitters, such as dopamine, we injected mice with a highly specific NET inhibitor atomoxetine (3 mg/kg i.p.) to inhibit the reuptake of NE. Although atomoxetine had no effect on the GRAB_{NE1m} peak fluorescence during the tail suspension test, it significantly slowed the return of signal to its baseline after each tail suspension (Figures 7F1, 7G1, 7H1, and 7I1); in contrast, treating mice with the α -adrenergic receptor antagonist yohimbine (2 mg/kg, i.p.) both decreased GRAB_{NE1m} peak fluorescence and significantly accelerated the return to baseline (Figures 7F1, 7G1, 7H1, and 7I1). Treating mice with either the selective DAT inhibitor GBR 12909 (10 mg/kg, i.p.) or the D2R antagonist sulpiride (50 mg/kg, i.p.) had no effect on the peak change in GRAB_{NE1m} fluorescence or the time to return to baseline (Figures 7F2, 7G2, 7H2, and 7I2). In summary, these data demonstrate that our GRAB_{NE} sensors are suitable for monitoring endogenous noradrenergic activity in real time, with high spatiotemporal precision, during freely moving behaviors in mammals.

DISCUSSION

Here, we report the development and validation of GRAB_{NE1m} and GRAB_{NE1h}, two genetically encoded NE sensors that can be used both *in vitro* and *in vivo* to monitor noradrenergic activity with high temporal and spatial resolution, high ligand specificity, and cell type specificity. In mouse acute brain slices, our GRAB_{NE} sensors detected NE release from the LC in response to electrical stimulation. In zebrafish, the GRAB_{NE} sensors reported looming-induced NE release with single-cell resolution. In mice, the GRAB_{NE} sensors reported time-locked release of NE in the LC triggered by optogenetic stimulation and in hypothalamic NE levels during a variety of stress-related behaviors.

Compared with the existing methods for measuring NE, our GRAB_{NE} sensors have distinct advantages. Our GRAB_{NE} sensors have extremely high specificity for NE over most other neurotransmitters and chemical modulators, including DA (Figures 2H and 3F). It has been difficult to distinguish NE from DA *in vivo* (e.g., by FSCV; Park et al., 2009; Robinson et al., 2003), largely because of their structural similarities: they differ in only one hydroxyl group. GRAB_{NE1m} has a roughly 1,000-fold-higher affinity for NE over DA when expressed in neurons, even better than the 85-fold difference of the wild-type α 2-adrenergic receptor. Thus,

our GRAB_{NE} sensors provide new opportunities to probe the dynamics of noradrenergic activity with high specificity, which is particularly valuable when studying the many brain regions that receive overlapping dopaminergic and noradrenergic inputs. A notable property of GRAB_{NE} sensors is their similar responses for NE and Epi. Almost all native human adrenergic receptors (α 1AR/1BR/1DR, α 2AR/2BR/2CR, and β 1R/2R/3R) also respond non-discriminately to both NE and Epi (1–10 μ M; Hoffman and Lefkowitz, 1980). So, from the target cells' perspective, GRAB_{NE} sensors provide a general tool to reveal when and where physiologically relevant levels of noradrenergic or adrenergic modulation occur. Discriminating NE versus Epi in the mammalian central nervous system is a relatively minor concern, because the specific enzyme (phenylethanolamine N-methyltransferase [PNMT]) that converts NE to Epi primarily exists in peripheral systems (e.g., adrenal medulla; Goldstein et al., 1972), except for very small groups of neurons in human brain (Kitahama et al., 1985).

Our GRAB_{NE} sensors have extremely high sensitivity for NE. Specifically, their EC₅₀ for NE spans sub-micromolar levels. Their dynamic range is high: 150%–230% mean increase in fluorescence intensity upon binding saturating NE. By comparison, recently published FRET-based NE indicators produce a signal change of $\leq 10\%$ under optimal conditions (Wang et al., 2018a, 2018b). Thus, GRAB_{NE} sensors have much improved characteristics for monitoring NE dynamics *in vivo*. Our sensors have brightness and photostability properties that rival EGFP, which permits stable recordings across extended experimental sessions. In addition, because they provide sub-second response kinetics and are genetically encoded, our GRAB_{NE} sensors can non-invasively report noradrenergic activity *in vivo* with single-cell resolution and high recording rate (~ 30 Hz). Moreover, because GRAB_{NE} sensors traffic to various surface membranes, including the cell body, dendrites, and axons, where they perform equally well, they are promising to provide subcellular spatial resolution, which is essential for understanding compartmental NE signaling *in vivo*. One caveat is that, because GRAB_{NE} sensors are engineered from the α 2A receptor, they may not be suitable for pharmacological investigation of α 2A-receptor-related regulation.

Ligand binding to endogenous GPCRs drives G-protein activation and receptor internalization. If recapitulated in GRAB_{NE} sensors, expression could interfere with endogenous signaling fidelity and disturb normal neuronal activity. We saw little

Figure 7. GRAB_{NE1m} Can Be Used to Measure Noradrenergic Activity in the Hypothalamus during Stress, Food-Related Behavior, and Social Interaction

(A) Schematic diagrams depicting the fiber photometry recording, virus injection, and recording sites.
 (B) Histology showing the expression of GRAB_{NE1m} (green) and placement of the recording; the nuclei were counterstained with DAPI (blue). Scale bar, 500 μ m.
 (C1–E6) Representative traces (C1–C6), average per-stimulus histograms (D1–D6), and summary data (E1–E6) showing normalized GRAB_{NE1m} fluorescence ($\Delta F/F$) before and during the forced swim test (1) and before, between, and during the tail suspension test (2), the hand presentation test (3), social interaction with an intruder of the opposite sex (4) and the same sex (5), and presentation of peanut butter (6). n = 3 animals each.
 (F) Representative traces of GRAB_{NE1m} fluorescence during the tail suspension test 10 min after saline injection, 25 min after atomoxetine (ATX) or YO injection, and 15 min after GBR 12909 or sulpiride (Sul) injection.

(G–I) Averaged peri-stimulus histograms (G), peak change in GRAB_{NE1m} fluorescence (H), and post-test decay time (I) measured during the tail suspension test after injection of the indicated compounds. n = 3 each.

The Shapiro-Wilk normality test was performed; if the test revealed it followed a normal distribution, a paired Student's t test or one-way repeated-measures ANOVA followed by Tukey's multiple comparisons was performed. If the values did not follow a normal distribution, a non-parametric ANOVA (Friedman's test) was performed followed by Dunn's multiple comparisons test. In (C) and (D), the blue dotted lines represent the start of the stimulus and the red dotted lines represent the end of the trial. *p < 0.05, **p < 0.01, and ***p < 0.001. See also Figure S6.

evidence of downstream coupling to both G-protein-independent and G-protein-dependent pathways. The introduction of the cpEGFP moiety in the GRAB_{NE} sensors resulted in undetectable engagement of arrestin-mediated desensitization and/or internalization, which suggests that the GRAB_{NE} sensors do not inadvertently activate arrestin-dependent signaling and ensures more consistent surface expression of the sensors. With respect to G-protein-dependent signaling, we found that, although physiological levels of NE robustly induce a change in GRAB_{NE} fluorescence, they do not significantly engage downstream G protein signaling (Figures 2J–2M).

Noradrenergic projections throughout the brain originate almost exclusively from the LC, and the released NE plays a role in a wide range of behaviors, including cognition and the regulation of arousal, attention, and alertness (Berridge and Waterhouse, 2003; Li et al., 2018; Schwarz et al., 2015). Interestingly, our fiber photometry recordings of GRAB_{NE} sensors' fluorescence in the hypothalamus of freely behaving mice revealed specific changes in noradrenergic activity under stressful, but not non-stressful, conditions. These data are generally consistent with previous data obtained using microdialysis to measure NE (Mc Quade and Stanford, 2000; Pacak et al., 1995; Shekhar et al., 2002; Tanaka, 1999). Nevertheless, it is worth noting that hypothalamus is a highly heterogeneous structure containing dozens of nuclei with diverse functions, it remains possible that NE is released during non-stressful conditions in regions outside of lateral hypothalamus. The spatial resolution and potential for cell type specificity of GRAB_{NE} sensors should enable more precise investigation of NE signaling across hypothalamic nuclei in freely moving animals.

NE circuits of the LC receive heterogeneous inputs from a broad range of brain regions and send heterogeneous outputs to many brain regions (Schwarz et al., 2015). Congruously, altered noradrenergic activity is associated with a broad range of psychiatric conditions and neurodegenerative diseases, including ADHD, PD, depression, and anxiety (Marien et al., 2004). The complexity of these disorders may, in part, reflect the complexity of noradrenergic circuits and signals, which cannot be fully dissected by previous tools. Therefore, the GRAB_{NE} sensors we present here are more suitable for understanding the regulation and impact of noradrenergic activity during complex behaviors. Deploying these in concert with other cell-specific tools for reporting (Jing et al., 2018; Patriarchi et al., 2018; Sun et al., 2018) and manipulating neurotransmitter levels (Fenno et al., 2011; Urban and Roth, 2015) will increase our understanding of the circuits and mechanisms that underlie brain functions in both health and disease.

STAR★METHODS

Detailed methods are provided in the online version of this paper and include the following:

- KEY RESOURCES TABLE
- CONTACT FOR REAGENT AND RESOURCE SHARING
- EXPERIMENTAL MODEL AND SUBJECT DETAILS
 - Primary cultures
 - Cell lines
 - Mice/Rats
 - Zebrafish

● METHOD DETAILS

- Molecular cloning
- Expression of GRAB_{NE} sensors in cultured cells and *in vivo*
- Fluorescence imaging of HEK293T cells and cultured neurons
- TANGO assay
- TGF α shedding assay
- FSCV
- Luciferase complementation assay
- Fluorescence imaging of GRAB_{NE} sensors in brain slices
- Electrophysiology
- Fluorescence imaging of zebrafish
- Fiber photometry recording in freely moving mice during optical stimulation
- Fiber photometry recording in mice during behavioral testing
- Behavioral assays

● QUANTIFICATION AND STATISTICAL ANALYSIS

● DATA AND SOFTWARE AVAILABILITY

SUPPLEMENTAL INFORMATION

Supplemental Information can be found with this article online at <https://doi.org/10.1016/j.neuron.2019.02.037>.

A video abstract is available at <https://doi.org/10.1016/j.neuron.2019.02.037#mmc4>.

ACKNOWLEDGMENTS

This work was supported by the National Basic Research Program of China (973 Program; grant 2015CB856402), the General Program of National Natural Science Foundation of China (project 31671118), the NIH BRAIN Initiative grant U01NS103558, the Junior Thousand Talents Program of China, the grants from the Peking-Tsinghua Center for Life Sciences and the State Key Laboratory of Membrane Biology at Peking University School of Life Sciences to Y.L.; the Key Research Program of Frontier Sciences (QZDY-SSW-SMC028) of Chinese Academy of Sciences and Shanghai Science and Technology Committee (18JC1410100) to J.D.; the NIH grants R01MH101377 and R21HD090563 and an Irma T. Hirsch Career Scientist Award to D.L.; the Intramural Research Program of the NIH/NIEHS of the United States (1ZIAES103310) to G.C.; and Peking University Postdoctoral Fellowship to Y.Z. J.J.Z. is the Radboud Professor and Sir Yue-Kong Pao Chair Professor. We thank Yi Rao for sharing the two-photon microscope and Xiaoguang Lei for the platform support of the Opera Phenix high-content screening system at PKU-CLS. We thank the Core Facilities at the School of Life Sciences, Peking University for assistance with DNA sequencing work, and we are grateful to Dr. Zhi Dong for his help of analyzing data. We thank Bryan Roth and Nevin Lambert for sharing stable cell lines and plasmids. We thank Yue Sun, Sunlei Pan, Lun Yang, and Haohong Li for inputs on sensors' characterization and application. We thank Yanhua Huang, Jianing Yu, Liqun Luo, and Mickey London for valuable feedback of the manuscript.

AUTHOR CONTRIBUTIONS

Y.L. conceived and supervised the project. J.F., M.J., H. Wang, A.D., and Z.W. performed experiments related to sensor development, optimization, and characterization in culture HEK cells, culture neurons, and brain slices. Y.Z., P.Z., and J.J.Z. designed and performed experiments using Sindbis virus in slices. C.Z., W.C., and J.D. designed and performed experiments on transgenic fish. J.E.L., J. Zhou, H. Wu, J. Zou, S.A.H., G.C., and D.L. designed and performed experiments in behaving mice. All authors contributed to data

interpretation and data analysis. Y.L. and J.F. wrote the manuscript with input from M.J., J.E.L., and D.L. and help from other authors.

DECLARATION OF INTERESTS

The authors declare competing financial interests. J.F., M.J., H. Wang, and Y.L. have filed patent applications whose value might be affected by this publication.

Received: October 5, 2018

Revised: January 28, 2019

Accepted: February 21, 2019

Published: March 25, 2019

REFERENCES

- Akerboom, J., Rivera, J.D.V., Guilbe, M.M.R., Malavé, E.C.A., Hernandez, H.H., Tian, L., Hires, S.A., Marvin, J.S., Looger, L.L., and Schreier, E.R. (2009). Crystal structures of the GCaMP calcium sensor reveal the mechanism of fluorescence signal change and aid rational design. *J. Biol. Chem.* **284**, 6455–6464.
- Akerboom, J., Chen, T.-W., Wardill, T.J., Tian, L., Marvin, J.S., Mutlu, S., Calderón, N.C., Esposti, F., Borghuis, B.G., Sun, X.R., et al. (2012). Optimization of a GCaMP calcium indicator for neural activity imaging. *J. Neurosci.* **32**, 13819–13840.
- Bast, N., Poustka, L., and Freitag, C.M. (2018). The locus coeruleus-norepinephrine system as pacemaker of attention - a developmental mechanism of derailed attentional function in autism spectrum disorder. *Eur. J. Neurosci.* **47**, 115–125.
- Berridge, C.W., and Spencer, R.C. (2016). Differential cognitive actions of norepinephrine α_2 and α_1 receptor signaling in the prefrontal cortex. *Brain Res.* **1641** (Pt B), 189–196.
- Berridge, C.W., and Waterhouse, B.D. (2003). The locus coeruleus-noradrenergic system: modulation of behavioral state and state-dependent cognitive processes. *Brain Res. Brain Res. Rev.* **42**, 33–84.
- Berridge, C.W., Schmeichel, B.E., and España, R.A. (2012). Noradrenergic modulation of wakefulness/arousal. *Sleep Med. Rev.* **16**, 187–197.
- Bito, L., Davson, H., Levin, E., Murray, M., and Snider, N. (1966). The concentrations of free amino acids and other electrolytes in cerebrospinal fluid, in vivo dialysate of brain, and blood plasma of the dog. *J. Neurochem.* **13**, 1057–1067.
- Brodde, O.-E., Bruck, H., Leineweber, K., and Seyfarth, T. (2001). Presence, distribution and physiological function of adrenergic and muscarinic receptor subtypes in the human heart. *Basic Res. Cardiol.* **96**, 528–538.
- Bruns, D. (2004). Detection of transmitter release with carbon fiber electrodes. *Methods* **33**, 312–321.
- Chefer, V.I., Thompson, A.C., Zapata, A., and Shippenberg, T.S. (2009). Overview of brain microdialysis. *Curr. Protoc. Neurosci., Chapter 7*, Unit7.1.
- Chrousos, G.P. (2009). Stress and disorders of the stress system. *Nat. Rev. Endocrinol.* **5**, 374–381.
- Chung, K.Y., Rasmussen, S.G., Liu, T., Li, S., DeVree, B.T., Chae, P.S., Calinski, D., Kobilka, B.K., Woods, V.L., Jr., and Sunahara, R.K. (2011). Conformational changes in the G protein Gs induced by the β_2 adrenergic receptor. *Nature* **477**, 611–615.
- Dugast, C., Cespuglio, R., and Suaud-Chagny, M.F. (2002). In vivo monitoring of evoked noradrenaline release in the rat anteroventral thalamic nucleus by continuous amperometry. *J. Neurochem.* **82**, 529–537.
- Espay, A.J., LeWitt, P.A., and Kaufmann, H. (2014). Norepinephrine deficiency in Parkinson's disease: the case for noradrenergic enhancement. *Mov. Disord.* **29**, 1710–1719.
- Falkner, A.L., Grosenick, L., Davidson, T.J., Deisseroth, K., and Lin, D. (2016). Hypothalamic control of male aggression-seeking behavior. *Nat. Neurosci.* **19**, 596–604.
- Fenko, L., Yizhar, O., and Deisseroth, K. (2011). The development and application of optogenetics. *Annu. Rev. Neurosci.* **34**, 389–412.
- Gibson, D.G., Young, L., Chuang, R.-Y., Venter, J.C., Hutchison, C.A., 3rd, and Smith, H.O. (2009). Enzymatic assembly of DNA molecules up to several hundred kilobases. *Nat. Methods* **6**, 343–345.
- Goddard, A.W., Ball, S.G., Martinez, J., Robinson, M.J., Yang, C.R., Russell, J.M., and Shekhar, A. (2010). Current perspectives of the roles of the central norepinephrine system in anxiety and depression. *Depress. Anxiety* **27**, 339–350.
- Goldstein, M., Fuxe, K., and Hökfelt, T. (1972). Characterization and tissue localization of catecholamine synthesizing enzymes. *Pharmacol. Rev.* **24**, 293–309.
- Hashikawa, K., Hashikawa, Y., Falkner, A., and Lin, D. (2016). The neural circuits of mating and fighting in male mice. *Curr. Opin. Neurobiol.* **38**, 27–37.
- Hoffman, B.B., and Lefkowitz, R.J. (1980). Radioligand binding studies of adrenergic receptors: new insights into molecular and physiological regulation. *Annu. Rev. Pharmacol. Toxicol.* **20**, 581–608.
- Inoue, A., Ishiguro, J., Kitamura, H., Arima, N., Okutani, M., Shuto, A., Higashiyama, S., Ohwada, T., Arai, H., Makide, K., and Aoki, J. (2012). TGF α shedding assay: an accurate and versatile method for detecting GPCR activation. *Nat. Methods* **9**, 1021–1029.
- Jing, M., Zhang, P., Wang, G., Feng, J., Mesik, L., Zeng, J., Jiang, H., Wang, S., Looby, J.C., Guagliardo, N.A., et al. (2018). A genetically encoded fluorescent acetylcholine indicator for in vitro and in vivo studies. *Nat. Biotechnol.* **36**, 726–737.
- Justice, J.B., Jr. (1993). Quantitative microdialysis of neurotransmitters. *J. Neurosci. Methods* **48**, 263–276.
- Kitahama, K., Pearson, J., Denoroy, L., Kopp, N., Ulrich, J., Maeda, T., and Jouvret, M. (1985). Adrenergic neurons in human brain demonstrated by immunohistochemistry with antibodies to phenylethanolamine-N-methyltransferase (PNMT): discovery of a new group in the nucleus tractus solitarius. *Neurosci. Lett.* **53**, 303–308.
- Kroeze, W.K., Sassano, M.F., Huang, X.-P., Lansu, K., McCorvy, J.D., Giguère, P.M., Sciaky, N., and Roth, B.L. (2015). PRESTO-Tango as an open-source resource for interrogation of the druggable human GPCRome. *Nat. Struct. Mol. Biol.* **22**, 362–369.
- Lee, G.J., Park, J.H., and Park, H.K. (2008). Microdialysis applications in neuroscience. *Neurol. Res.* **30**, 661–668.
- Leibowitz, S.F. (1970). Reciprocal hunger-regulating circuits involving alpha- and beta-adrenergic receptors located, respectively, in the ventromedial and lateral hypothalamus. *Proc. Natl. Acad. Sci. USA* **67**, 1063–1070.
- Leibowitz, S.F., Jhanwar-Uniyal, M., Dvorkin, B., and Makman, M.H. (1982). Distribution of α -adrenergic, β -adrenergic and dopaminergic receptors in discrete hypothalamic areas of rat. *Brain Res.* **233**, 97–114.
- Li, L., Feng, X., Zhou, Z., Zhang, H., Shi, Q., Lei, Z., Shen, P., Yang, Q., Zhao, B., Chen, S., et al. (2018). Stress accelerates defensive responses to looming in mice and involves a locus coeruleus-superior colliculus projection. *Curr. Biol.* **28**, 859–871.e5.
- Lin, D., Boyle, M.P., Dollar, P., Lee, H., Lein, E.S., Perona, P., and Anderson, D.J. (2011). Functional identification of an aggression locus in the mouse hypothalamus. *Nature* **470**, 221–226.
- Manglik, A., Kim, T.H., Masureel, M., Altenbach, C., Yang, Z., Hilger, D., Lerch, M.T., Kobilka, T.S., Thian, F.S., Hubbell, W.L., et al. (2015). Structural insights into the dynamic process of β_2 -adrenergic receptor signaling. *Cell* **161**, 1101–1111.
- Marien, M.R., Colpaert, F.C., and Rosenquist, A.C. (2004). Noradrenergic mechanisms in neurodegenerative diseases: a theory. *Brain Res. Brain Res. Rev.* **45**, 38–78.
- Marvin, J.S., Borghuis, B.G., Tian, L., Cichon, J., Harnett, M.T., Akerboom, J., Gordus, A., Renninger, S.L., Chen, T.W., Bargmann, C.I., et al. (2013). An optimized fluorescent probe for visualizing glutamate neurotransmission. *Nat. Methods* **10**, 162–170.
- McQuade, R., and Stanford, S.C. (2000). A microdialysis study of the noradrenergic response in rat frontal cortex and hypothalamus to a conditioned cue for aversive, naturalistic environmental stimuli. *Psychopharmacology (Berl.)* **148**, 201–208.

- Meng, C., Zhou, J., Papaneri, A., Peddada, T., Xu, K., and Cui, G. (2018). Spectrally resolved fiber photometry for multi-component analysis of brain circuits. *Neuron* 98, 707–717.e4.
- Moore, R.Y., and Bloom, F.E. (1979). Central catecholamine neuron systems: anatomy and physiology of the norepinephrine and epinephrine systems. *Annu. Rev. Neurosci.* 2, 113–168.
- Moret, C., and Briley, M. (2011). The importance of norepinephrine in depression. *Neuropsychiatr. Dis. Treat.* 7 (Suppl 1), 9–13.
- Muller, A., Joseph, V., Slesinger, P.A., and Kleinfeld, D. (2014). Cell-based reporters reveal in vivo dynamics of dopamine and norepinephrine release in murine cortex. *Nat. Methods* 11, 1245–1252.
- Nakanishi, J., Takarada, T., Yunoki, S., Kikuchi, Y., and Maeda, M. (2006). FRET-based monitoring of conformational change of the β_2 adrenergic receptor in living cells. *Biochem. Biophys. Res. Commun.* 343, 1191–1196.
- Nygaard, R., Zou, Y., Dror, R.O., Mildorf, T.J., Arlow, D.H., Manglik, A., Pan, A.C., Liu, C.W., Fung, J.J., Bokoch, M.P., et al. (2013). The dynamic process of $\beta(2)$ -adrenergic receptor activation. *Cell* 152, 532–542.
- Olive, M.F., Mehmert, K.K., and Hodge, C.W. (2000). Microdialysis in the mouse nucleus accumbens: a method for detection of monoamine and amino acid neurotransmitters with simultaneous assessment of locomotor activity. *Brain Res. Brain Res. Protoc.* 5, 16–24.
- Pacak, K., Palkovits, M., Kopin, I.J., and Goldstein, D.S. (1995). Stress-induced norepinephrine release in the hypothalamic paraventricular nucleus and pituitary-adrenocortical and sympathoadrenal activity: in vivo microdialysis studies. *Front. Neuroendocrinol.* 16, 89–150.
- Park, J., Kile, B.M., and Wightman, R.M. (2009). In vivo voltammetric monitoring of norepinephrine release in the rat ventral bed nucleus of the stria terminalis and anteroventral thalamic nucleus. *Eur. J. Neurosci.* 30, 2121–2133.
- Patriarchi, T., Cho, J.R., Merten, K., Howe, M.W., Marley, A., Xiong, W.-H., Folk, R.W., Broussard, G.J., Liang, R., Jang, M.J., et al. (2018). Ultrafast neuronal imaging of dopamine dynamics with designed genetically encoded sensors. *Science* 360, eaat4422.
- R Development Core Team. (2016). R: A Language and Environment for Statistical Computing. R Foundation for Statistical Computing, Vienna.
- Rasmussen, S.G., Choi, H.J., Fung, J.J., Pardon, E., Casarosa, P., Chae, P.S., Devree, B.T., Rosenbaum, D.M., Thian, F.S., Kobilka, T.S., et al. (2011a). Structure of a nanobody-stabilized active state of the $\beta(2)$ adrenoceptor. *Nature* 469, 175–180.
- Rasmussen, S.G., DeVree, B.T., Zou, Y., Kruse, A.C., Chung, K.Y., Kobilka, T.S., Thian, F.S., Chae, P.S., Pardon, E., Calinski, D., et al. (2011b). Crystal structure of the β_2 adrenergic receptor-Gs protein complex. *Nature* 477, 549–555.
- Ren, Q., Kurose, H., Lefkowitz, R.J., and Cotecchia, S. (1993). Constitutively active mutants of the alpha 2-adrenergic receptor. *J. Biol. Chem.* 268, 16483–16487.
- Robinson, D.L., Venton, B.J., Heien, M.L.A.V., and Wightman, R.M. (2003). Detecting subsecond dopamine release with fast-scan cyclic voltammetry in vivo. *Clin. Chem.* 49, 1763–1773.
- Robinson, D.L., Hermans, A., Seipel, A.T., and Wightman, R.M. (2008). Monitoring rapid chemical communication in the brain. *Chem. Rev.* 108, 2554–2584.
- Schwarz, L.A., and Luo, L. (2015). Organization of the locus coeruleus-norepinephrine system. *Curr. Biol.* 25, R1051–R1056.
- Schwarz, L.A., Miyamichi, K., Gao, X.J., Beier, K.T., Weissbourd, B., DeLoach, K.E., Ren, J., Ibanes, S., Malenka, R.C., Kremer, E.J., and Luo, L. (2015). Viral-genetic tracing of the input-output organization of a central noradrenergic circuit. *Nature* 524, 88–92.
- Shekhar, A., Katner, J.S., Sajdyk, T.J., and Kohl, R.R. (2002). Role of norepinephrine in the dorsomedial hypothalamic panic response: an in vivo microdialysis study. *Pharmacol. Biochem. Behav.* 71, 493–500.
- Singleman, C., and Holtzman, N.G. (2014). Growth and maturation in the zebrafish, *Danio rerio*: a staging tool for teaching and research. *Zebrafish* 11, 396–406.
- Sokolowski, K., and Corbin, J.G. (2012). Wired for behaviors: from development to function of innate limbic system circuitry. *Front. Mol. Neurosci.* 5, 55.
- Sun, F., Zeng, J., Jing, M., Zhou, J., Feng, J., Owen, S.F., Luo, Y., Li, F., Wang, H., Yamaguchi, T., et al. (2018). A genetically encoded fluorescent sensor enables rapid and specific detection of dopamine in flies, fish, and mice. *Cell* 174, 481–496.e19.
- Tanaka, M. (1999). Emotional stress and characteristics of brain noradrenergic release in the rat. *Ind. Health* 37, 143–156.
- Urban, D.J., and Roth, B.L. (2015). DREADDs (designer receptors exclusively activated by designer drugs): chemogenetic tools with therapeutic utility. *Annu. Rev. Pharmacol. Toxicol.* 55, 399–417.
- Vilardaga, J.-P., Bünemann, M., Krasel, C., Castro, M., and Lohse, M.J. (2003). Measurement of the millisecond activation switch of G protein-coupled receptors in living cells. *Nat. Biotechnol.* 21, 807–812.
- Wan, Q., Okashah, N., Inoue, A., Nehmé, R., Carpenter, B., Tate, C.G., and Lambert, N.A. (2018). Mini G protein probes for active G protein-coupled receptors (GPCRs) in live cells. *J. Biol. Chem.* 293, 7466–7473.
- Wang, G., Wyskiel, D.R., Yang, W., Wang, Y., Milbern, L.C., Lalanne, T., Jiang, X., Shen, Y., Sun, Q.-Q., and Zhu, J.J. (2015). An optogenetics- and imaging-assisted simultaneous multiple patch-clamp recording system for decoding complex neural circuits. *Nat. Protoc.* 10, 397–412.
- Wang, A., Feng, J., Li, Y., and Zou, P. (2018a). Beyond fluorescent proteins: hybrid and bioluminescent indicators for imaging neural activities. *ACS Chem. Neurosci.* 9, 639–650.
- Wang, H., Jing, M., and Li, Y. (2018b). Lighting up the brain: genetically encoded fluorescent sensors for imaging neurotransmitters and neuromodulators. *Curr. Opin. Neurobiol.* 50, 171–178.
- Watson, C.J., Venton, B.J., and Kennedy, R.T. (2006). In vivo measurements of neurotransmitters by microdialysis sampling. *Anal. Chem.* 78, 1391–1399.
- Yang, T., and Shah, N.M. (2016). Molecular and neural control of sexually dimorphic social behaviors. *Curr. Opin. Neurobiol.* 38, 89–95.
- Yao, Y., Li, X., Zhang, B., Yin, C., Liu, Y., Chen, W., Zeng, S., and Du, J. (2016). Visual cue-discriminative dopaminergic control of visuomotor transformation and behavior selection. *Neuron* 89, 598–612.
- Yizhar, O., Fenno, L.E., Prigge, M., Schneider, F., Davidson, T.J., O’Shea, D.J., Sohal, V.S., Goshen, I., Finkelstein, J., Paz, J.T., et al. (2011). Neocortical excitation/inhibition balance in information processing and social dysfunction. *Nature* 477, 171–178.
- Yusa, K., Zhou, L., Li, M.A., Bradley, A., and Craig, N.L. (2011). A hyperactive piggyBac transposase for mammalian applications. *Proc. Natl. Acad. Sci. USA* 108, 1531–1536.
- Zhang, L., Zhang, P., Wang, G., Zhang, H., Zhang, Y., Yu, Y., Zhang, M., Xiao, J., Crespo, P., Hell, J.W., et al. (2018). Ras and Rap signal bidirectional synaptic plasticity via distinct subcellular microdomains. *Neuron* 98, 783–800.e4.
- Zhao, Y., Araki, S., Wu, J., Teramoto, T., Chang, Y.-F., Nakano, M., Abdelfattah, A.S., Fujiwara, M., Ishihara, T., Nagai, T., and Campbell, R.E. (2011). An expanded palette of genetically encoded Ca^{2+} indicators. *Science* 333, 1888–1891.
- Zhou, Z., and Misler, S. (1995). Amperometric detection of stimulus-induced quantal release of catecholamines from cultured superior cervical ganglion neurons. *Proc. Natl. Acad. Sci. USA* 92, 6938–6942.
- Zimmerman, B.G. (1981). Adrenergic facilitation by angiotensin: does it serve a physiological function? *Clin. Sci. (Lond.)* 60, 343–348.
- Zou, P., Zhao, Y., Douglass, A.D., Hochbaum, D.R., Brinks, D., Werley, C.A., Harrison, D.J., Campbell, R.E., and Cohen, A.E. (2014). Bright and fast multi-coloured voltage reporters via electrochromic FRET. *Nat. Commun.* 5, 4625.

STAR★METHODS

KEY RESOURCES TABLE

REAGENT or RESOURCE	SOURCE	IDENTIFIER
Antibodies		
Chicken polyclonal anti-GFP antibody	Abcam	Cat#ab13970; RRID: AB_300798
Rabbit polyclonal anti-Dopamine beta Hydroxylase (DBH) antibody	Abcam	Cat#ab209487
Alexa 488-conjugated goat-anti-chicken IgG (H+L)	Invitrogen	Cat#A11039; RRID: AB_142924
Alexa-555-conjugated goat-anti-rabbit IgG (H+L)	AAT Bioquest	Cat#16690
DAPI fluoromount-G	SouthernBiotech	Cat#0100-20
Bacterial and Virus Strains		
Sindbis-NE1m	This paper	N/A
Sindbis-NE1h	This paper	N/A
Sindbis-NEmut	This paper	N/A
AAV9-hSyn-NE1m	Vigene Biosciences	N/A
AAV9-hSyn-NE1h	Vigene Biosciences	N/A
AAV9-Ef1a-DIO-C1V1-YFP	Gift from Karl Deisseroth; Yizhar et al., 2011	Addgene viral prep # 35497-AAV9; RRID: Addgene_35497
AAV9-hSyn-NEmut	Vigene Biosciences	N/A
AAV9-hsyn-tTA	Vigene Biosciences	N/A
AAV9-TRE-NE1h	Vigene Biosciences	N/A
AAV9-hSyn-DA1m	Vigene Biosciences	N/A
Chemicals, Peptides, and Recombinant Proteins		
Norepinephrine bitartrate (NE)	Sigma-Aldrich	Cat#A9512
UK 14,304 tartrate (UK or brimonidine)	Tocris	Cat#2466
Yohimbine hydrochloride (YO)	Tocris	Cat#1127
Epinephrine hydrochloride (Epi)	Sigma-Aldrich	Cat#E4642
Isoprenaline hydrochloride (ISO)	Sigma-Aldrich	Cat#15627
ICI 118,551 hydrochloride (ICI)	Sigma-Aldrich	Cat#1127
Dopamine hydrochloride (DA)	Sigma-Aldrich	Cat#H8502
Haloperidol hydrochloride (Halo)	Tocris	Cat#0931
Serotonin hydrochloride (5-HT)	Tocris	Cat#3547
Histamine dihydrochloride (His)	Tocris	Cat#3545
L-Glutamic acid (Glu)	Sigma-Aldrich	Cat#V900408
γ -Aminobutyric acid (GABA)	Tocris	Cat#0344
Adenosine (ADO)	Tocris	Cat#3624
Acetylcholine chloride (ACh)	Solarbio	Cat#G8320
Tyramine (TA)	Sigma-Aldrich	Cat#V900670
NPEC-caged-noradrenaline (NPEC-caged-NE)	Santa Cruz	Cat#sc-361279
Desipramine hydrochloride (Desi)	Sigma-Aldrich	Cat#D3900
GBR 12909 (GBR)	Tocris	Cat#0421
Eticlopride hydrochloride (Etic)	Tocris	Cat#1847
Atomoxetine hydrochloride (ATX)	Sigma-Aldrich	Cat#Y0001586
Sulpiride	Sigma-Aldrich	Cat#s8010
2,2,2-Tribromoethanol (Avetin)	Sigma-Aldrich	Cat#T48402
α -bungarotoxin	Tocris	Cat#2133
Low melting-point agarose	Sigma-Aldrich	Cat#A9414

(Continued on next page)

Continued

REAGENT or RESOURCE	SOURCE	IDENTIFIER
T5-exonuclease	New England Biolabs	Cat#M0363S
Phusion DNA polymerase	Thermo Fisher Scientific	Cat#F530L
Taq ligase	iCloning	Cat#TDL-100
Cal590	AAT Bioquest	Cat#20510
Critical Commercial Assays		
NanoLuc Luciferase Assay	Promega	Cat#N1110
Experimental Models: Cell Lines		
HEK293T	ATCC	Cat#CRL-3216; RRID: CVCL_0063
HTLA cells for tango assay	Gift from Bryan L. Roth; Kroeze et al., 2015	N/A
HEK293T cell line stably expressing chimeric $G\alpha q/i$ and AP-TGF α	Inoue et al., 2012	N/A
HEK293T cell line stably expressing NE1m, chimeric $G\alpha q/i$ and AP-TGF α	This paper	N/A
HEK293T cell line stably expressing wt- $\alpha 2AR$, chimeric $G\alpha q/i$ and AP-TGF α	This paper	N/A
Experimental Models: Organisms/Strains		
Mouse: wild-type Sprague-Dawley rat pups (P0)	Beijing Vital River Laboratory Animal Technology Co., Ltd.	http://www.vitalriver.com/
Mouse: wild-type C57BL/6	Beijing Vital River Laboratory Animal Technology Co., Ltd.	http://www.vitalriver.com/
Mouse: wild-type C57BL/6	Charles River Laboratories	https://www.criver.com/
Mouse: B6.FVB(Cg)-Tg(Th-cre)Fl172Gsat/Mmucd	MMRRC	RRID: MMRRC_031029-UCD
Zebrafish: albino (slc45a2 ^{b4}) (The background strain)	ZFIN	N/A
Zebrafish: Tg(HuC:GRAB _{NE1m})	This paper	N/A
Zebrafish: Tg(HuC:GRAB _{NE1h})	This paper	N/A
Zebrafish: Tg(HuC:GRAB _{NEmut})	This paper	N/A
Zebrafish: Tg(HuC:NES-jRGECO1a)	This paper	N/A
Zebrafish: Tg(HuC:NES-jRGECO1a);Tg(HuC:GRAB _{NE1m})	This paper	N/A
Oligonucleotides		
PCR primers	This paper	See Table S1
Recombinant DNA		
pDisplay vector	Invitrogen	Cat#V66020
pDisplay-NE1m-IRES-mCherry-CAAX	This paper	N/A
pDisplay-NE1h-IRES-mCherry-CAAX	This paper	N/A
pDisplay-NEmut-IRES-mCherry-CAAX	This paper	N/A
pDisplay-NE0.5 m-IRES-mCherry-CAAX	This paper	N/A
pAAV-TRE-NE1h	This paper	N/A
pAAV-hSyn-tTA	This paper	N/A
Full-length human GPCR cDNAs	human ORFeome 8.1	http://horfdb.dfci.harvard.edu/
pDisplay- $\alpha 2AR$ -EGFP(ICL3)-IRES-mCherry-CAAX	This paper	N/A
pDisplay- $\alpha 2AR$ -cpEGFP(ICL3)-IRES-mCherry-CAAX	This paper	N/A
pDisplay- $\alpha 1DR$ -cpEGFP(ICL3)-IRES-mCherry-CAAX	This paper	N/A
pDisplay- $\alpha 2BR$ -cpEGFP(ICL3)-IRES-mCherry-CAAX	This paper	N/A
pDisplay- $\beta 2R$ -cpEGFP(ICL3)-IRES-mCherry-CAAX	This paper	N/A
pDisplay- $\beta 3R$ -cpEGFP(ICL3)-IRES-mCherry-CAAX	This paper	N/A
pDest-mScarlet-CAAX	This paper	N/A
pDest-EGFP-CAAX	This paper	N/A
pDest-KDEL1-EGFP	This paper	N/A

(Continued on next page)

Continued

REAGENT or RESOURCE	SOURCE	IDENTIFIER
pDest-PSD95-mScarlet	This paper	N/A
pDest-Synaptophysin-mScarlet	This paper	N/A
pPacific- α 2AR (for cell line construction)	This paper	N/A
pPacific-NE1m (for cell line construction)	This paper	N/A
pTango- α 2AR	This paper	N/A
pTango-NE1m	This paper	N/A
pTango-NE1h	This paper	N/A
pCS7-PiggyBAC	IEWSOLID BIOTECH; Yusa et al., 2011	N/A
pCS7-PiggyBAC (S103P, S509G)	This paper	N/A
LgBit-mGsi	Gift from Nevin A. Lambert; Wan et al., 2018	N/A
α 2AR-SmBit	This paper	N/A
NE1m-SmBit	This paper	N/A
NE1h-SmBit	This paper	N/A
pTol2-HuC:GRAB _{NE1m}	This paper	N/A
pTol2-HuC:GRAB _{NE1h}	This paper	N/A
pTol2-HuC:GRAB _{NEmut}	This paper	N/A
Tol2 mRNA	This paper	N/A
Software and Algorithms		
ImageJ	NIH	https://imagej.nih.gov/ij/ ; RRID: SCR_003070
Origin 9.1	OriginLab	https://www.originlab.com/
MATLAB	MathWorks	https://www.mathworks.com/products/matlab.html ; RRID: SCR_001622
Arduino	Arduino	https://www.arduino.cc
GraphPad Prism 7	GraphPad Software	RRID: SCR_002798
R	R Development Core Team, 2016	RRID: SCR_001905
Linear Spectral Unmixing Algorithm v1.1	NIH	https://www.niehs.nih.gov/research/atniehs/labs/ln/pi/iv/tools/index.cfm
Other		
Microsyringe pumps for virus injection	WPI/Drummond Scientific	Nanoliter 2000 Injector/Nanoject II
Inverted confocal microscope	Nikon	Ti-E A1
Inverted confocal microscope	Olympus	FV3000
Upright confocal microscope	Olympus	FV1000
Opera Phenix high content screening system	PerkinElmer	Cat#HH14000000
Multilabel plate reader	PerkinElmer	VICTOR X5
Tethered FSCV system	Pinnacle Technology	Pinnacle tethered
Vibratome	Leica	VT1200
Cryostat	Leica	CM1900
Two-photon microscope	Olympus	FV1000MPE
Mai Tai Ti:Sapphire laser	Spectra-Physics	Deepsee
Patch clamp amplifier	Molecular Devices	Axopatch-200B
Concentric electrode	FHC	#CBAEC75
Optical fibers	Thorlabs	BFH48-400
Ceramic ferrule	Thorlabs	SFLC440-10
Blue LED light	Thorlabs	M470F1

(Continued on next page)

Continued

REAGENT or RESOURCE	SOURCE	IDENTIFIER
Blue LED driver	Thorlabs	LEDD1B
Femtowatt Silicon Photoreceiver	Newport	2151
BioAmp processor	TDT	RZ5
Slide scanner microscope	Olympus	VS120

CONTACT FOR REAGENT AND RESOURCE SHARING

Further information and requests for resources and reagents should be directed to and will be fulfilled by the Lead Contact, Yulong Li (Yulongli@pku.edu.cn).

EXPERIMENTAL MODEL AND SUBJECT DETAILS**Primary cultures**

Rat cortical neurons were prepared from postnatal day 0 (P0) Sprague-Dawley rat pups (both male and female, randomly selected; Beijing Vital River). In brief, cortical neurons were dissociated from dissected P0 rat brains in 0.25% Trypsin-EDTA (GIBCO), plated on 12-mm glass coverslips coated with poly-D-lysine (Sigma-Aldrich), and cultured at 37°C in 5% CO₂ in neurobasal medium (GIBCO) containing 2% B-27 supplement, 1% GlutaMax, and 1% penicillin-streptomycin (GIBCO).

Cell lines

HEK293T cells were obtained from ATCC (CRL-3216) and verified based on their morphology under the microscope and by their growth curve. Stable cell lines expressing the wild-type $\alpha 2$ -adrenergic receptor or various GRAB_{NE} sensors were constructed by co-transfecting cells with the pPiggyBac plasmid carrying target genes with Tn5 transposase into a stable HEK293T-based cell line expressing chimeric G α q/i and AP-TGF α (Inoue et al., 2012). Cells that stably expressed the target genes were selected by treating with 2 mg/ml Puromycin (Sigma) after reaching 100% confluence. The HTLA cells used for the TANGO assay stably express a tTA-dependent luciferase reporter and a β -arrestin2-TEV fusion gene and were a gift from Bryan L. Roth (Kroeze et al., 2015). All cell lines were cultured at 37°C in 5% CO₂ in DMEM (GIBCO) supplemented with 10% (v/v) fetal bovine serum (GIBCO) and 1% penicillin-streptomycin (GIBCO).

Mice/Rats

All procedures regarding animals were approved by the respective Animal Care and Use Committees at Peking University, New York University, University of Southern California, University of Virginia and the US National Institutes of Health and were performed in compliance with the US National Institutes of Health guidelines for the care and use of laboratory animals. Wild-type Sprague-Dawley rat pups (P0) were used to prepare cultured cortical neurons and pups (P6-7) were used to prepare cultured hippocampal slices. Wild-type C57BL/6 and Th-Cre mice (MMRRC_031029-UCD, obtained from MMRRC) were used to prepare the acute brain slices and for the *in vivo* mouse experiments. Experimental Th-Cre mice were produced by breeding Th-Cre hemizygous BAC transgenic mice with C57BL/6J mice. All animals were housed in the animal facility and were family-housed or pair-housed in a temperature-controlled room with a 12hr-12h light-dark cycle (10 pm to 10 am light) with food and water provided *ad libitum*. All *in vivo* mouse experiments were performed using 2-12-month-old mice of both sexes.

Zebrafish

The background strain for these experiments is the albino strain *slc45a2*^{b4}. To generate transgenic zebrafish, both the pTol2-HuC:GRAB_{NE1m} plasmid and Tol2 mRNA were co-injected into single-cell stage zebrafish eggs, and the founders of Tg(HuC:GRAB_{NE1m}) were screened at adult stage. Tg(HuC:GRAB_{NE1h}) and Tg(HuC:GRAB_{NEmut}) were generated as described above by using the pTol2-HuC:GRAB_{NE1h} and pTol2-HuC:GRAB_{NEmut} plasmid, respectively. Adult fish and larvae were maintained on a 14h-10h light-dark cycle at 28°C. All experimental larvae were raised to 6-8 days post-fertilization (dpf) in 10% Hank's solution, which consisted of (in mM): 140 NaCl, 5.4 KCl, 0.25 Na₂HPO₄, 0.44 KH₂PO₄, 1.3 CaCl₂, 1.0 MgSO₄, and 4.2 NaHCO₃ (pH 7.2). Larval zebrafish do not undergo sex differentiation prior to 1 month post-fertilization (Singleman and Holtzman, 2014).

METHOD DETAILS**Molecular cloning**

The molecular clones used in this study were generated by Gibson Assembly (Gibson et al., 2009) using DNA fragments amplified using primers (Thermo Fisher Scientific, Table S1) with 25-bp overlap. The Gibson Assembly cloning enzymes consisted of T5-exonuclease (New England Biolabs), Phusion DNA polymerase (Thermo Fisher Scientific), and Taq ligase (iCloning). Sanger sequencing was performed using the sequencing platform at the School of Life Sciences of Peking University in order to verify

the sequence of all clones. All cDNAs encoding the candidate GRAB_{NE} sensors were cloned into the pDisplay vector (Invitrogen) with an upstream IgK leader sequence and a downstream IRES-mCherry-CAAX cassette to label the cell membrane. The cDNAs of select adrenergic receptor candidates were amplified from the human GPCR cDNA library (hORFeome database 8.1), and cpEGFP from GCaMP6s was inserted into the third intracellular loop (ICL3). The insertion sites for the GRAB_{NE} sensors were screened by truncating the ICL3 of the α 2-adrenergic receptor at the 10-amino acid (AA) level, followed by fine-tuning at the 1-AA level. Coupling linkers were randomized by PCR amplification using randomized NNB codons in target sites. Other cDNAs used to express the GRAB_{NE} sensors in neurons were cloned into the pAAV vector using the human synapsin promoter (hSyn) or TRE promoter. pAAV-hSyn-tTA was used to drive expression of the TRE promoter. The plasmids carrying compartmental markers were cloned by fusing EGFP-CAAX, RFP-CAAX (mScarlet), KDEL-EGFP, PSD95-RFP, and synaptophysin-RFP into the pDest vector. The sensors were also subcloned into Sindbis viral vector for cultured hippocampal slices expression. To characterize signaling downstream of the GRAB_{NE} sensors, we cloned the sensors and the wild-type α 2-adrenergic receptor into the pTango and pPiggyBac vector, respectively. A hyperactive piggyBac transposase was generated by introducing two mutations into pCS7-PiggyBAC (VIEWSOLID BIOTECH) (Yusa et al., 2011). GRAB_{NE1m}-SmBit and α 2AR-SmBit constructs were derived from β 2AR-SmBit (Wan et al., 2018) using a BamHI site incorporated upstream of the GGSG linker. LgBit-mGsi was a gift from Nevin A. Lambert.

Expression of GRAB_{NE} sensors in cultured cells and *in vivo*

The GRAB_{NE} sensors were characterized in HEK293T cells and cultured rat cortical neurons, with the exception of the TANGO assay and TGF α shedding assay. HEK293T cells were passaged with Trypsin-EDTA (0.25%, phenol red; GIBCO) and plated on 12-mm size 0 glass coverslips in 24-well plates and grown to ~70% confluence for transfection. HEK293T cells were transfected by incubating cells with a mixture containing 1 μ g of DNA and 3 μ g of PEI for 6 h. Imaging was performed 24–48 h after transfection. Cells expressing GRAB_{NE} sensors for screening were plated on 96-well plates (PerkinElmer).

Cultured neurons were transfected using the calcium phosphate method at 7–9 DIV. In brief, the neurons were incubated for 2 h in a mixture containing 125 mM CaCl₂, HBS (pH 7.04), and 1.5 μ g DNA. The DNA-Ca₃(PO₄)₂ precipitate was then removed from the cells by washing twice with warm HBS (pH 6.80). Cells were imaged 48 h after transfection.

For *in vivo* expression, the mice were anesthetized by an i.p. injection of 2,2,2-tribromoethanol (Avetin, 500 mg/kg body weight, Sigma-Aldrich) or under isoflurane anesthesia, and then placed in a stereotaxic frame for injection of AAVs using a Nanoliter 2000 Injector (WPI) or Nanoject II (Drummond Scientific) microsyringe pump. For the experiments shown in Figures 4, 6, and S4J–S4M, the AAVs containing hSyn-GRAB_{NE1m/NE1h/NEmut/DA1m} and Ef1a-DIO-C1V1-YFP (Yizhar et al., 2011) were injected into the LC (AP: –5.45 mm relative to Bregma; ML: \pm 1.25 mm relative to Bregma; and DV: –2.25 mm from the brain surface) or SNc (AP: –3.1 mm relative to Bregma; ML: \pm 1.5 mm relative to Bregma; and DV: –3.8 mm from the brain surface) of wild-type or Th-Cre mice. For experiments shown in Figures S4A–S4I, AAVs containing hSyn-tTA and TRE-GRAB_{NE1h} were injected into the dentate gyrus (AP: –1.8 mm relative to Bregma; ML: \pm 0.8 mm relative to Bregma; and DV: –2.0 mm from the brain surface) of wild-type mice. For the experiments shown in Figures 7 and S6, 100 nL of AAV9-hSyn-GRAB_{NE1m} or AAV9-hSyn-GRAB_{NEmut} (Vigene, 1×10^{13} titer genomic copies per ml) were unilaterally into the hypothalamus (AP: –1.7 mm relative to Bregma; ML: 0.90 mm relative to Bregma; and DV: –6.05 mm from the brain surface) of wild-type (C57BL/6) mice at a rate of 10 nl/min.

Fluorescence imaging of HEK293T cells and cultured neurons

HEK293T cells and cultured neurons expressing GRAB_{NE} sensors were screened using an Opera Phenix high-content imaging system (PerkinElmer) and imaged using an inverted Ti-E A1 confocal microscope (Nikon). A 60x/1.15 NA water-immersion objective was mounted on the Opera Phenix and used to screen GRAB_{NE} sensors with a 488-nm laser and a 561-nm laser. A 525/50 nm and a 600/30 nm emission filter were used to collect the GFP and RFP signals, respectively. HEK293T cells expressing GRAB_{NE} sensors were first bathed in Tyrode's solution and imaged before and after addition of the indicated drugs at the indicated concentrations. The change in fluorescence intensity of the GRAB_{NE} sensors was calculated using the change in the GFP/RFP ratio. For confocal microscopy, the microscope was equipped with a 40x/1.35 NA oil-immersion objective, a 488-nm laser, and a 561-nm laser. A 525/50 nm and a 595/50 nm emission filter were used to collect the GFP and RFP signals, respectively. GRAB_{NE}-expressing HEK293T cells and neurons were perfused with Tyrode's solutions containing the drug of interest in the imaging chamber. The photostability of GRAB_{NE} sensors and EGFP was measured using a confocal microscope (for 1-photon illumination) equipped with a 488-nm laser at a power setting of ~350 μ W, and using a FV1000MPE 2-photon microscope (Olympus, 2-photon illumination) equipped with a 920-nm laser at a power setting of ~27.5 mW. The illuminated region was the entire HEK293T cell expressing the target protein, with an area of ~200 μ m². Photolysis of 100 μ M NPEC-caged-NE (Santa Cruz) was performed by combining fast scanning with a 76-ms pulse of 405-nm laser illumination by a confocal microscope. 10 μ M YO was used to specifically block the NE-induced fluorescence response. 100 μ M NE and 200 μ M yohimbine were used in determination of on or off kinetics in rapid perfusion experiments.

TANGO assay

NE at various concentrations (ranging from 0.1 nM to 100 μ M) was applied to α 2AR-expressing or GRAB_{NE1m}-/GRAB_{NE1h}-expressing HTLA cells (Kroeze et al., 2015). The cells were then cultured for 12 h to allow expression of the luciferase gene. Furimazine (NanoLuc Luciferase Assay, Promega) was then applied to a final concentration of 5 μ M, and luminescence was measured using a VICTOR X5 multilabel plate reader (PerkinElmer).

TGF α shedding assay

TGF shedding assay was performed as previously described (Inoue et al., 2012). Stable cell lines expressing G α i-AP-TGF α together with the wild-type α 2AR or GRAB_{NE1m} were plated in a 96-well plate and treated by the addition of 10 μ L of a 10x solution of NE in each well, yielding a final NE concentration ranging from 0.1 nM to 100 μ M. Absorbance at 405 nm was read using a VICTOR X5 multi-label plate reader (PerkinElmer). TGF α release was calculated as described previously (Inoue et al., 2012). Relative levels of G protein activation were calculated as the TGF α release of GRAB_{NE} sensors normalized to the release mediated by wild-type α 2AR.

FSCV

Fast-scan cyclic voltammetry (FSCV) was performed using 7- μ m carbon fiber microelectrodes. Voltammograms were measured with a triangular potential waveform from -0.4 V to $+1.1$ V at a scan rate of 400 V/s with a 100-ms interval. The carbon fiber microelectrode was held at -0.4 V between scans. Voltammograms measured in the presence of various different drugs in Tyrode's solution were generated using the average of 200 scans followed by the subtraction of the average of 200 background scans. Currents were recorded using the Pinnacle tethered FSCV system (Pinnacle Technology). Pseudocolor plots were generated using Pinnacle FSCV software.

Luciferase complementation assay

The luciferase complementation assay was performed as previously described (Wan et al., 2018). In brief, \sim 48h after transfection the cells were washed with PBS, harvested by trituration, and transferred to opaque 96-well plates containing diluted NE solutions from 1 nM to 100 μ M. Furimazine (NanoLuc Luciferase Assay, Promega) was added to each well immediately prior to performing the measurements with Nluc.

Fluorescence imaging of GRAB_{NE} sensors in brain slices

Fluorescence imaging of acute brain slices was performed as previously described (Sun et al., 2018). In brief, the animals were anesthetized with Avertin, and acute brain slices containing the LC region or the hippocampus region were prepared in cold slicing buffer containing (in mM): 110 choline-Cl, 2.5 KCl, 1.25 NaH₂PO₄, 25 NaHCO₃, 7 MgCl₂, 25 glucose, and 2 CaCl₂. Slices were allowed to recover at 35°C in oxygenated Ringers solution containing (in mM): 125 NaCl, 2.5 KCl, 1.25 NaH₂PO₄, 25 NaHCO₃, 1.3 MgCl₂, 25 glucose, and 2 CaCl₂ for at least 40 min before experiments. An Olympus FV1000MPE two-photon microscope equipped with a 40x/0.80 NA water-immersion objective and a mode-locked Mai Tai Ti:Sapphire laser (Spectra-Physics) tuned to 920 nm were used for imaging the slices. For electrical stimulation, a concentric electrode (model #CBAEC75, FHC) was positioned near the LC region, and the imaging and stimuli were synchronized using an Arduino board controlled using a custom-written program. The imaging speed was set at 0.148 s/frame with 128 \times 96 pixels in each frame. The stimulation voltage was set at \sim 6 V, and the duration of each stimulation was typically 1 ms. Drugs were either delivered via the perfusion system or directly bath-applied in the imaging chamber. For the calcium imaging experiments, the acute brain slices expressing GRAB_{NE1h} were prepared and bath loaded with red calcium dye Cal590 (20 μ M, AAT Bioquest Inc., Sunnyvale, CA) for 1h, and subsequently washed in ACSF for 30 mins before conducting two-photon imaging. Cal590 dye was excited with two-photon laser at 920 nm, and 90 mM KCl was perfused to stimulate calcium signals.

For immunostaining of brain sections, GRAB_{NE}-expressing mice were anesthetized with Avertin, and the heart was perfused with 0.9% NaCl followed by 4% paraformaldehyde (PFA). The brain was then removed, placed in 4% PFA for 4 h, and then cryoprotected in 30% (w/v) sucrose for 24 h. The brain was embedded in tissue-freezing medium, and 50- μ m thick coronal sections were cut using a Leica CM1900 cryostat (Leica, Germany). A chicken anti-GFP antibody (1:500, Abcam, #ab13970) was used to label GRAB_{NE}, and a rabbit anti-DBH antibody (1:50, Abcam, #ab209487) was used to label adrenergic terminals in the hippocampus. Alexa 488-conjugated goat-anti-chicken and Alexa-555-conjugated goat-anti-rabbit secondary antibodies were used, and the nuclei were counterstained with DAPI. The sections were imaged using a confocal microscope (Nikon).

Electrophysiology

Cultured slices were prepared from P6–7 rats following the previous studies (Wang et al., 2015; Zhang et al., 2018). In brief, the hippocampus were dissected out in ice-cold HEPES-buffered Hanks' solution (pH 7.35) under sterile conditions, sectioned into 400 μ m slices on a tissue chopper, and explanted onto a Millicell-CM membrane (0.4- μ m pore size; Millipore, MA). The membranes were then placed in 750 μ L of MEM culture medium, contained (in mM): HEPES 30, heat-inactivated horse serum 20%, glutamine 1.4, D-glucose 16.25, NaHCO₃ 5, CaCl₂ 1, MgSO₄ 2, insulin 1 mg/ml, ascorbic acid 0.012% at pH 7.28 and osmolarity 320. Cultured slices were maintained at 35°C, in a humidified incubator (ambient air enriched with 5% CO₂).

Simultaneous dual whole-cell recordings were obtained from two nearby infected and non-infected hippocampal CA1 pyramidal neurons under visual guidance using fluorescence and transmitted light illumination. The patch recording pipettes (4–7 M Ω) were filled with intracellular solution 120 mM potassium gluconate, 4 mM KCl, 10 mM HEPES, 4 mM MgATP, 0.3 mM Na₃GTP, 10 mM sodium phosphocreatine and 0.5% biocytin (pH 7.25) for voltage-clamp recordings. Bath solution (29 \pm 1.5°C) contained (in mM): NaCl 119, KCl 2.5, CaCl₂ 4, MgCl₂ 4, NaHCO₃ 26, NaH₂PO₄ 1 and glucose 11, at pH 7.4 and gassed with 5% CO₂/95% O₂. Whole-cell recordings were made with up to two Axopatch-200B patch clamp amplifiers (Molecular Devices, Sunnyvale, CA).

Fluorescence imaging of zebrafish

Tg(HuC:GRAB_{NE1m}) and Tg(HuC:GRAB_{NE1h}) zebrafish larvae were imaged by using an upright confocal microscope (Olympus FV1000, Japan) equipped with a 20x/0.95 NA water-dipping objective. The larvae were first paralyzed with α -bungarotoxin (100 μ g/ml, Sigma), mounted dorsal side up in 1.5% low melting-point agarose (Sigma), and then perfused with an extracellular solution consisting of (in mM) 134 NaCl, 2.9 KCl, 4 CaCl₂, 10 HEPES, and 10 glucose (290 mOsmol/L, pH 7.8). Images were acquired at 1–2 Hz with a view field of 800 \times 800 pixels and a voxel size was 0.62 \times 0.62 \times 2.0 μ m³ (x \times y \times z). To detect the sensor's response to exogenous NE, 50 μ M L-(-)-norepinephrine (+)-bitartrate salt monohydrate (Sigma) in 5 μ M L-ascorbic acid and 50 μ M yohimbine hydrochloride (TOCRIS) were sequentially applied to the bath. To detect endogenous NE release, visual looming stimuli, which mimic approaching objects or predators (Yao et al., 2016) were projected to the larvae under a red background. Each trial lasted 5 s, and 5 trials were performed in a block, with a 90 s interval between trials. To examine the specificity of responses, ICI 118,551 hydrochloride (50 μ M, Sigma), yohimbine hydrochloride (50 μ M, TOCRIS), and desipramine hydrochloride (50 μ M, Sigma) were applied. Looming stimuli in transiently transfected HuC:GRAB_{NE1m} zebrafish were measured at single-cell resolution by using the same conditions described above. To examine whether overexpression of GRAB_{NE} sensors affect neuronal activities, we performed spontaneous and looming-evoked calcium imaging for tectal neurons in Tg(HuC:NES-jRGECO1a) with or without HuC:GRAB_{NE1m} expression. Ten minutes' spontaneous calcium activities were recorded after 15-min habituation.

Fiber photometry recording in freely moving mice during optical stimulation

In the all-optic experiments shown in Figure 6, multimode optical fiber probes (105/125 μ m core/cladding) were implanted into the LC (AP: -5.45 mm relative to Bregma; ML: ± 0.85 mm relative to Bregma; and DV: -3.5 mm from the brain surface) and the SNc (AP: -3.1 mm relative to Bregma; ML: ± 1.5 mm relative to Bregma; and DV: -3.85 mm from the brain surface) in mice four weeks after viral injection. Fiber photometry recording in the LC and/or SNc was performed using a 473-nm laser with an output power of 25 μ W measured at the end of the fiber. The measured emission spectra were fitted using a linear unmixing algorithm (<https://www.niehs.nih.gov/research/atniehs/labs/ln/pi/iv/tools/index.cfm>). The coefficients generated by the unmixing algorithm were used to represent the fluorescence intensities of various fluorophores (Meng et al., 2018). To evoke C1V1-mediated NE/DA release, pulse trains (10-ms pulses at 20 Hz for 1 s) were delivered to the LC/SNc using a 561-nm laser with an output power of 9.9 mW measured at the end of the fiber.

Fiber photometry recording in mice during behavioral testing

For the experiments in Figures 7 and S6, a fiber photometry recording set-up was generated and used as previously described (Falkner et al., 2016). GRAB_{NE1m} was injected into the lateral hypothalamus (Bregma AP: -1.7 mm; ML: 0.90 mm; DV: -6.05 mm) of C57BL/6 mice in a volume of 100 nL containing AAV9-hSyn-GRAB_{NE1m} (Vigene, 1×10^{13} titer genomic copies per ml) or AAV9-hSyn-GRAB_{NEmut} (Vigene, 1×10^{13} titer genomic copies per ml) at 10 nl/min. A 400- μ m optic fiber (Thorlabs, BFH48-400) housed in a ceramic ferrule (Thorlabs, SFLC440-10) was implanted 0.2 mm above the injection site. The virus was left to incubate for three weeks. Prior to fiber photometry recording, a ferrule sleeve was used to connect a matching optic fiber to the implanted fiber. For recordings, a 400-Hz sinusoidal blue LED light (30 μ W; M470F1 driven by an LEDD1B driver; both from Thorlabs) was bandpass-filtered (passing band: 472 ± 15 nm, Semrock, FF02-472/30-25) and delivered to the brain in order to excite GRAB_{NE1m}. The emission light passed through the same optic fiber, through a bandpass filter (passing band: 534 ± 25 nm, Semrock, FF01-535/50), and into a Femtowatt Silicon Photoreceiver, which recorded the GRAB_{NE1m} emission using an RZ5 real-time processor (Tucker-Davis Technologies). The 400-Hz signals from the photoreceiver were extracted in real time using a custom-written program (Tucker-Davis Technologies) and used to reflect the intensity of the GRAB_{NE1m} fluorescence signal.

Behavioral assays

All behavioral tests were performed at least 1 h after the onset of the dark cycle. For the tail suspension test, each mouse was gripped by the tail and lifted off the bottom of its cage six times for 60 s each, with at least 1 min between each lift. For the forced swim test, the mouse was gently placed in a 1000 mL conical flask containing lukewarm water and removed after 4–6 min. After removal from the water, the mouse was gently dried with paper towels and placed in the home cage on a heating pad. For conspecific assays, an adult C57BL/6 group-housed mouse of either sex was placed inside the test mouse's cage for 10 min. No sexual behavior or aggressive behavior was observed during the interaction. For the food assay, ~ 4 g of peanut butter was placed in the cap of a 15 mL plastic tube and placed inside of the test mouse's cage for 10 min. During that period, the test mouse was free to explore, sniff, and eat the peanut butter. All videos were acquired at 25 frames per second and manually annotated frame-by-frame using a custom MATLAB program (Lin et al., 2011). "Approach" refers to the period in which the subject mouse walks toward the intruder mouse. "Sniff" refers to the time in which the subject mouse sniffs the conspecific intruder. "Being sniffed" refers to the period in which the subject mouse is being sniffed by the conspecific intruder. "Contact" with the social stimulus refers to the period in which the test mouse sniffed or was sniffed by the intruder. "Contact" with the peanut butter refers to the period in which the test mouse sniffed or ate the peanut butter. "Lift" refers to the period in which the experimenter gripped the mouse's tail and lifted the mouse into the air.

QUANTIFICATION AND STATISTICAL ANALYSIS

For the imaging experiments using cultured HEK293T cells, primary neurons, and brain slices, images were first imported to ImageJ software (National Institutes of Health) for fluorescence intensity readouts, and then analyzed using MATLAB (MathWorks) with a custom-written script or Origin Pro (OriginLab). The fluorescence response traces in the brain slices shown in [Figure 4](#) were processed with 3x binning and then plotted.

Time-lapse images of the zebrafish were analyzed using Fiji to acquire the fluorescence intensity in the region of interest (ROI) in each frame. A custom-written MATLAB program was then used to calculate the change in fluorescence intensity ($\Delta F/F_0$) as $(F_t - F_0)/F_0$, where F_t was the fluorescence intensity at time t and F_0 was the average fluorescence intensity during the entire time window. Statistical analyses were performed using GraphPad Prism 6 and Origin Pro (OriginLab).

For the fiber photometry data shown in [Figure 7](#), the MATLAB function “msbackadj” with a moving window of 25% of the total recording duration was first applied to obtain the instantaneous baseline signal (F_{baseline}). The instantaneous $\Delta F/F$ was calculated as $(F_{\text{raw}} - F_{\text{baseline}})/F_{\text{baseline}}$, and a peri-stimulus histogram (PSTH) was calculated by aligning the $\Delta F/F$ signal of each trial to the onset of the behavior of interest. The response elicited during a behavior was calculated as the average $\Delta F/F$ during all trials of a given behavior. The response between behavioral periods was calculated as the average $\Delta F/F$ between two behavioral episodes excluding 4 s immediately before the behavior’s onset, as some uncontrolled and/or unintended events (e.g., chasing the animal before the tail suspension test) may have occurred during that period. The baseline signal was calculated as the average $\Delta F/F$ 100 s prior to the start of the behavioral test. The peak response after each drug injection was calculated as the average maximum $\Delta F/F$ during all tail suspension trials. The decay time was calculated as the average time required to reach half of the peak response.

Except where indicated otherwise, group differences were analyzed using the Student’s t test, Wilcoxon matched-pairs signed rank test, Shapiro-Wilk normality test, one-way ANOVA test, or Friedman’s test. Except where indicated otherwise, all summary data are presented as the mean \pm SEM.

DATA AND SOFTWARE AVAILABILITY

The custom-written MATLAB programs using in this study will be provided upon request to the corresponding author.

Neuron, Volume 102

Supplemental Information

A Genetically Encoded Fluorescent Sensor for Rapid and Specific *In Vivo* Detection of Norepinephrine

Jiesi Feng, Changmei Zhang, Julieta E. Lischinsky, Miao Jing, Jingheng Zhou, Huan Wang, Yajun Zhang, Ao Dong, Zhaofa Wu, Hao Wu, Weiyu Chen, Peng Zhang, Jing Zou, S. Andrew Hires, J. Julius Zhu, Guohong Cui, Dayu Lin, Jiulin Du, and Yulong Li

Fig S1

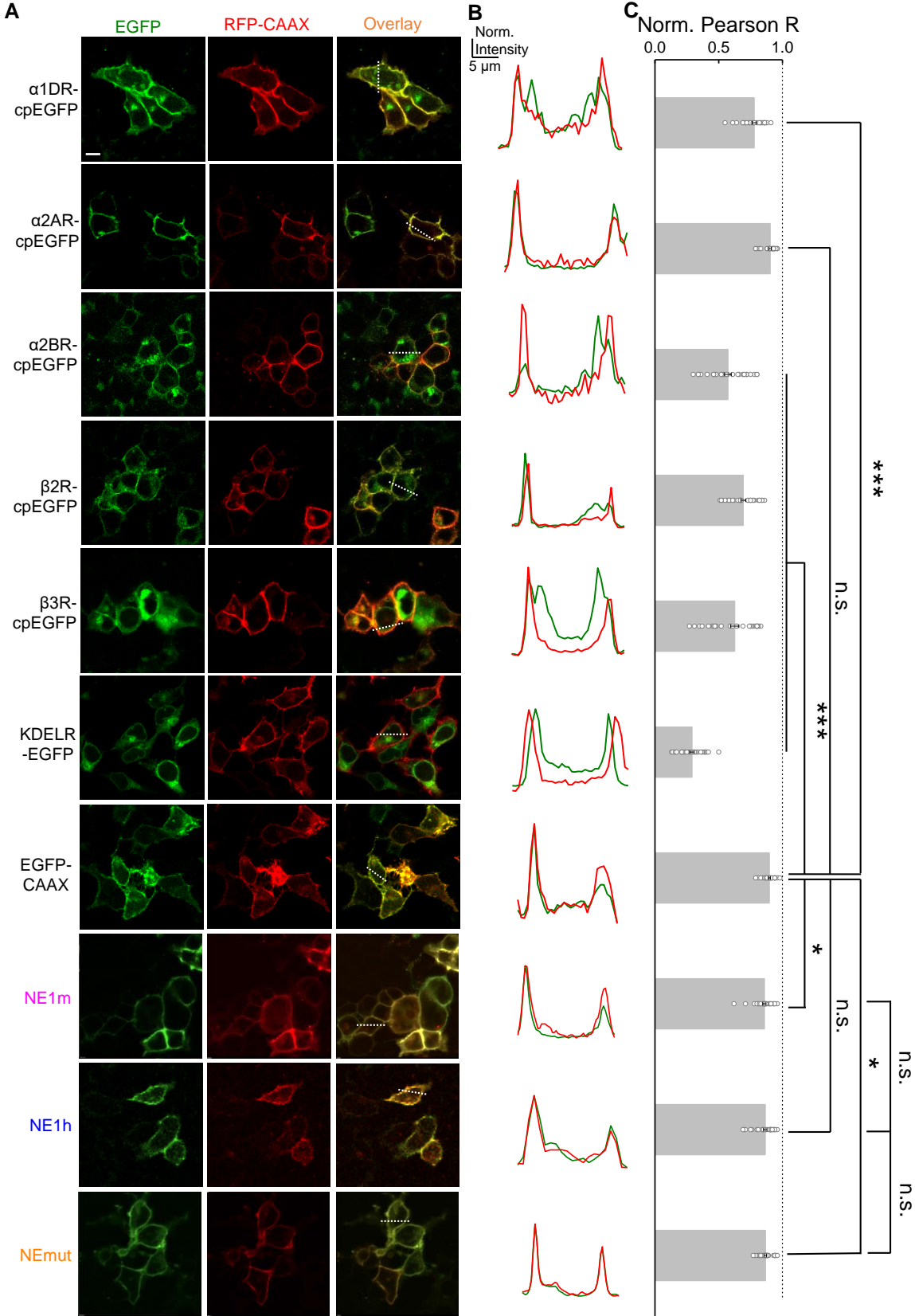


Fig S2

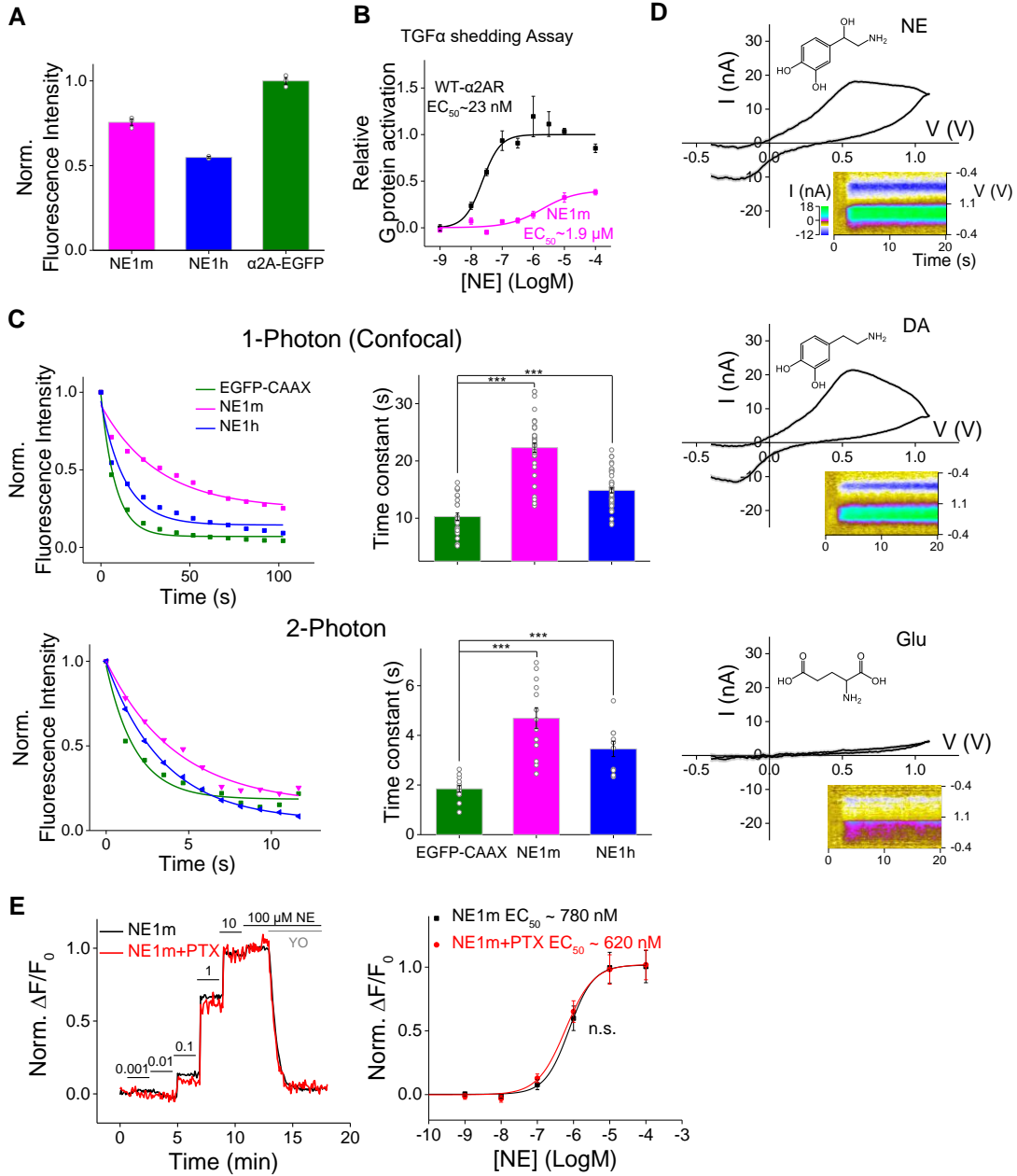


Fig S3

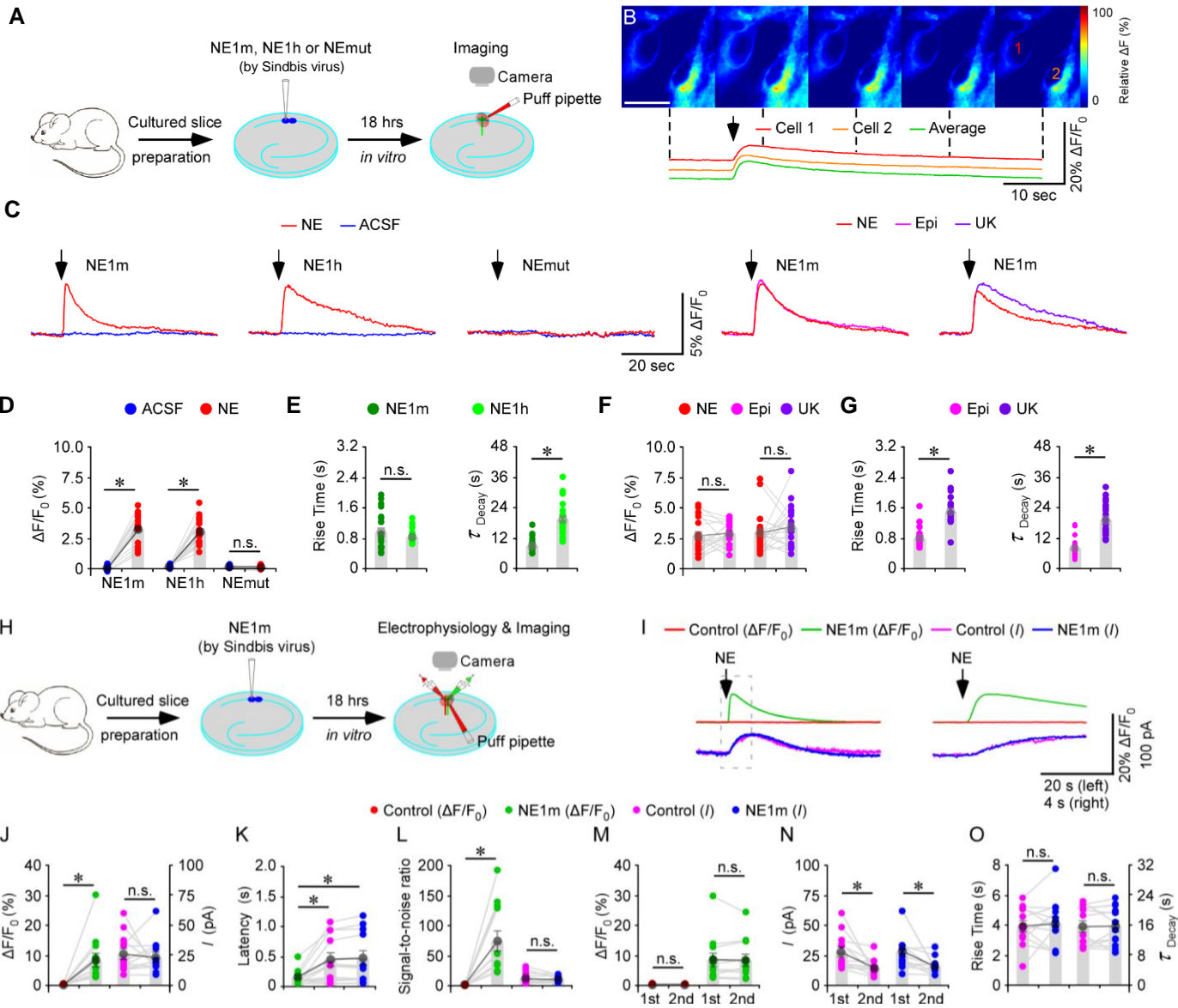


Fig S4

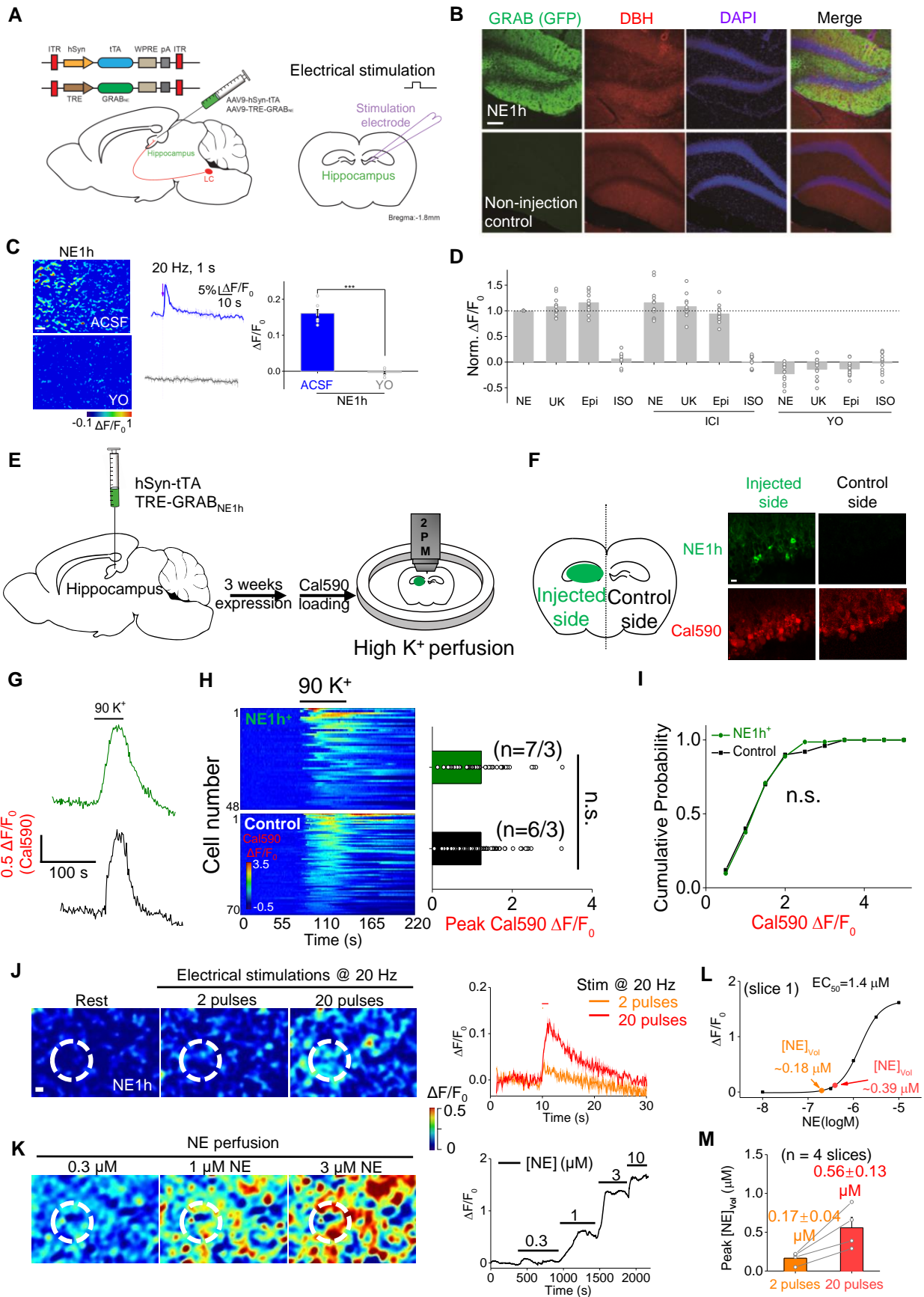


Fig S5

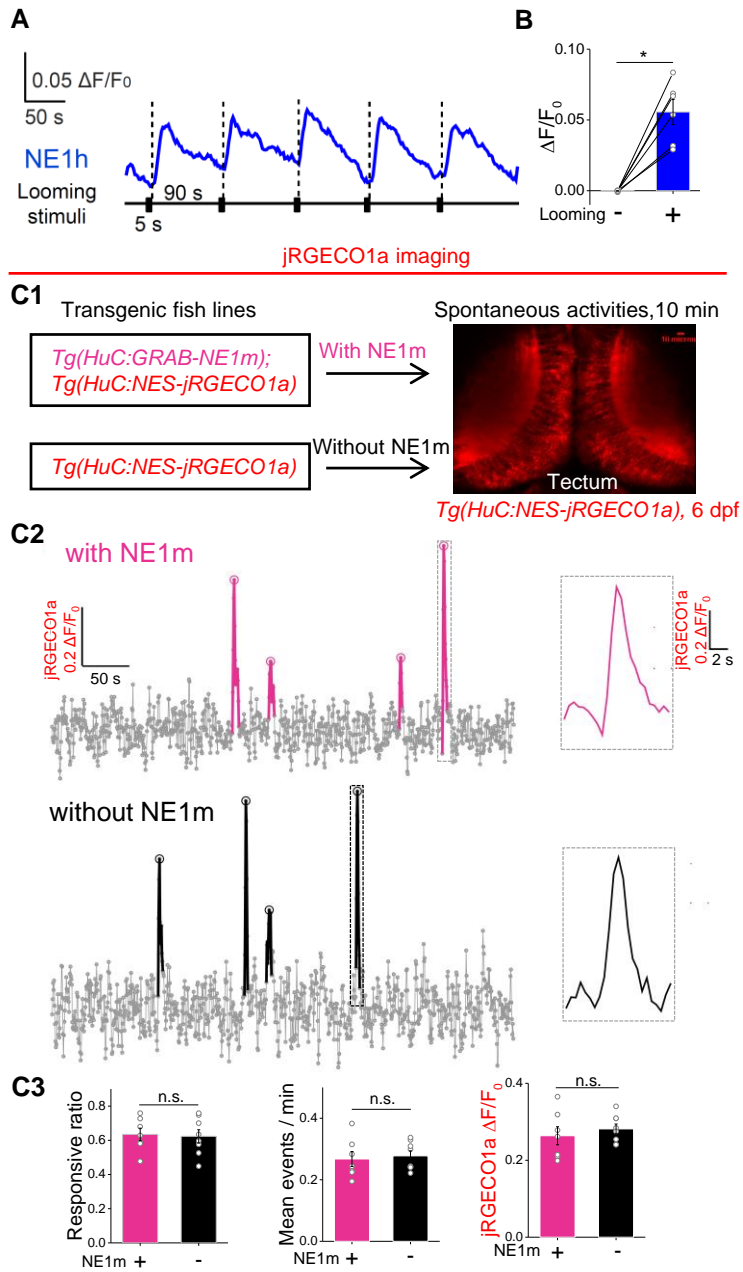
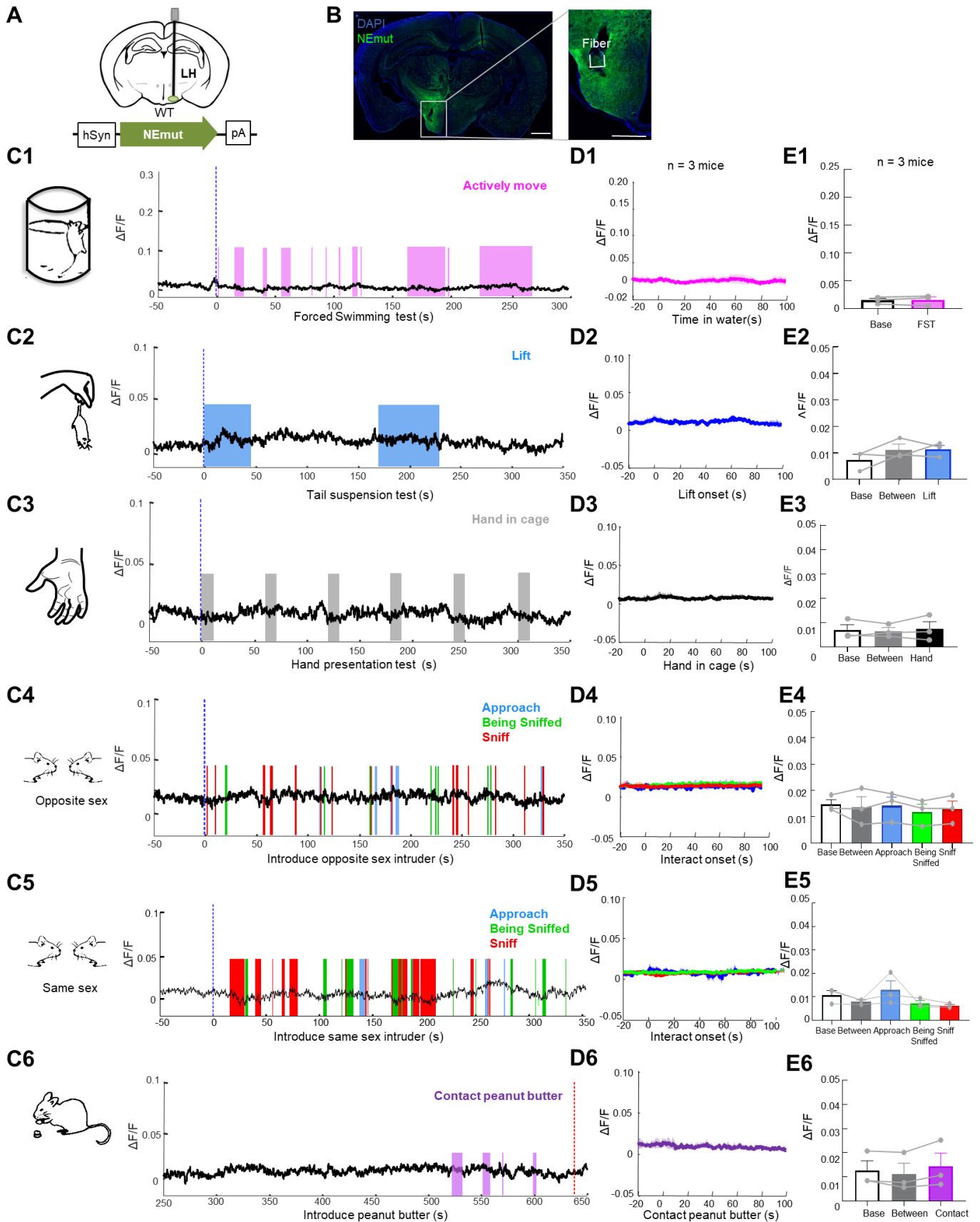


Fig S6



1 **Figure S1. Characterization of the membrane trafficking of a panel of screening**
2 **candidates, related to Figure 1.**

3 Representative images (**A**) of HEK293T cells co-transfected with the indicated screening
4 candidates (green) together with RFP-CAAX (red) to label the plasma membrane. KDELR-
5 EGFP was used as an ER marker. The dashed white lines indicate the line used for the
6 line-scanning data shown in (**B**) and summarized in

7 (**C**) $n = 30$ cells from 4-5 cultures.

8 The scale bars in (**A**) represent $10\ \mu\text{m}$.

9 $*p < 0.05$ and $***p < 0.001$; n.s., not significant (Student's t -test).

10

11 **Figure S2. Further characterization of GRAB_{NE} sensors, related to Figure 2 and**
12 **Figure 3.**

13 **(A)** Fluorescence intensity of GRAB_{NE1m} and GRAB_{NE1h} expressed relative to EGFP- α 2AR.
14 $n \geq 2$ wells with 300-500 cells per well.

15 **(B)** G protein activation mediated by GRAB_{NE1m} and wild-type α 2AR was measured using
16 the TGF α shedding assay and is expressed relative to α 2AR. $n = 4$ wells with $\geq 10^5$ cells
17 per well.

18 **(C)** Exemplar **(left)** and summary data **(right)** showing the photostability of GRAB_{NE}
19 sensors and EGFP-CAAX using confocal **(top)** and 2-photon **(bottom)** microscopy. $n > 10$
20 cells from at least 3 cultures.

21 **(D)** Exemplar cyclic voltammograms for 10 μ M NE **(top)**, 10 μ M DA **(middle)**, and 10 μ M
22 Glu **(bottom)** measured using FSCV are shown. The traces were averaged from separate
23 200 trials.

24 **(E)** Disrupting of G protein activation with pertussis toxin does not affect the NE-induced
25 fluorescence change in GRAB_{NE1m}-expressing neurons. $n = 27$ neurons from 3 cultures.

26 *** $p < 0.001$ (Student's t -test).

27

28 **Figure S3. GRAB_{NE} sensors respond selectively to noradrenergic agonists in brain**

29 **lices without affecting endogenous NE receptor functions, related to Figure 4.**

30 (A) Schematic drawing showing the experimental design for measuring CA1 pyramidal
31 neurons in cultured rat hippocampal slices.

32 (B) Heat-map images of the change in fluorescence in GRAB_{NE1m}-expressing CA1 neurons
33 in response to a 10-ms local application of NE (20 μ M). The red and orange traces show
34 the fluorescence responses of two neurons, and the green trace shows the average
35 response of all neurons in the field.

36 (C) Fluorescence responses measured in GRAB_{NE1m}⁻, GRAB_{NE1h}⁻, and GRAB_{NEmut}⁻
37 expressing CA1 neurons following a 10-ms puff (arrow) of ACSF, NE (20 μ M), Epi (100
38 μ M), or brimonidine (UK, 20 μ M).

39 (D) Maximum $\Delta F/F_0$ responses measured in GRAB_{NE1m}⁻, GRAB_{NE1h}⁻, and GRAB_{NEmut}⁻
40 expressing CA1 neurons following a 10-ms puff of ACSF or NE. $n = 20-21$ cells from 8
41 animals per group.

42 (E) Rise times and decay time constants measured in CA1 neurons expressing GRAB_{NE1m}⁻
43 and GRAB_{NE1h}⁻ expressing CA1 neurons in response to a puff of NE. $n = 21$ cells from 8
44 animals.

45 (F) Maximum $\Delta F/F_0$ responses measured in GRAB_{NE1m}-expressing CA1 neurons following
46 a puff of NE, Epi, or brimonidine (UK). $n = 20-21$ cells from 8 animals per group.

47 (G) Rise times and decay time constants measured in GRAB_{NE1m}-expressing CA1 neurons
48 following a puff of Epi or brimonidine (UK).

49 (H) Schematic drawing outlines the design of simultaneous imaging and
50 electrophysiological recording experiments in rat cultured hippocampal slices.

51 (I) Left, simultaneous fluorescence and current responses of a pair of GRAB_{NE1m}
52 expressing and neighboring control non-expressing CA1 neurons to a 10-ms puff
53 application of 0.2 mM norepinephrine (NE). Right, the responses in the left rectangle box
54 are shown again in an expanded time scale. Note the different latencies of fluorescence
55 and current responses.

56 (J) Values for the amplitude of noradrenergic fluorescence (GRAB_{NE1m}: $8.52 \pm 2.26\%$; Ctrl:
57 $0.14 \pm 0.02\%$; $Z = 3.059$; $p = 0.002$; $n = 12$ from 12 animals) and current (GRAB_{NE1m}: 23.4
58 ± 4.2 pA; Ctrl: 26.4 ± 4.7 pA; $Z = 0.078$; $p = 0.937$; $n = 12$ from 12 animals) responses of
59 GRAB_{NE1m} expressing CA1 neurons compared to non-expressing neurons.

60 (K) Values for the latency of noradrenergic current responses in GRAB_{NE1m} expressing
61 (GRAB_{NE1m}: 462.0 ± 124.2 ms; $Z = 2.578$; $p = 0.01$) and non-expressing CA1 neurons (Ctrl:
62 440.6 ± 113.1 ms; $Z = 2.432$; $p = 0.015$) compared to those of fluorescence responses of

63 GRAB_{NE1m} expressing neurons (GRAB_{NE1m}: 145.8 ± 36.4 ms; $n = 12$ from 12 animals).

64 **(L)** Values for the signal-to-noise ratio (SNR) of noradrenergic fluorescence responses of
65 GRAB_{NE1m} expressing CA1 neurons compared to non-expressing neurons (GRAB_{NE1m}:
66 75.9 ± 17.1 ; Ctrl: 2.5 ± 0.3 ; $Z = 3.509$; $p = 0.002$; $n = 12$ from 12 animals) and noradrenergic
67 current responses of GRAB_{NE1m} expressing CA1 neurons compared to non-expressing
68 neurons (GRAB_{NE1m}: 9.6 ± 1.6 ; Ctrl: 11.3 ± 2.8 ; $Z = -0.235$; $p = 0.814$; $n = 12$ from 12 animals).
69 Note the larger SNR of noradrenergic fluorescence responses of GRAB_{NE1m} expressing
70 CA1 neurons compared to current responses of GRAB_{NE1m} expressing and non-expressing
71 CA1 neurons (GRAB_{NE1m}: $Z = -3.509$; $p = 0.002$; Ctrl: $Z = -2.981$; $p = 0.002$).

72 **(M)** Values for the two consecutive fluorescence responses of GRAB_{NE1m} expressing (1st:
73 $8.56 \pm 0.02\%$; 2nd: $8.43 \pm 0.02\%$; $Z = 0$; $p = 1$; $n = 12$ from 12 animals) and control non-
74 expressing (1st: $0.14 \pm 0.02\%$; 2nd: $0.11 \pm 0.01\%$; $Z = -1.832$; $p = 0.067$; $n = 12$ from 12
75 animals) CA1 neurons.

76 **(N)** Values for the two consecutive noradrenergic current responses in GRAB_{NE1m}
77 expressing (1st: 28.6 ± 5.0 pA; 2nd: 15.6 ± 2.0 pA; $Z = -2.51$; $p = 0.012$; $n = 12$ from 12
78 animals) and control non-expressing (1st: 27.7 ± 4.4 pA; 2nd: 14.9 ± 2.0 pA; $Z = -3.059$;
79 $p = 0.02$; $n = 12$ from 12 animals) CA1 neurons.

80 **(O)** Values for the rise time (GRAB_{NE1m}: 4.14 ± 0.46 s; Ctrl: 3.98 ± 0.38 s; $Z = 0.314$; $p =$
81 0.754 ; $n = 12$ from 12 animals) and decay time constant (GRAB_{NE1m}: 15.81 ± 1.50 s; Ctrl:
82 15.70 ± 1.53 s; $Z = 0.784$; $p = 0.433$; $n = 12$ from 12 animals) of noradrenergic current
83 responses in GRAB_{NE1m} expressing neurons compared to control non-expressing CA1
84 neurons. Large gray dots indicate average responses and asterisks indicate $p < 0.05$
85 (Wilcoxon tests).
86
87

88 **Figure S4. GRAB_{NE} sensors respond selectively to noradrenergic agonists in brain**
89 **slices without disturbing neuronal activities, related to Figure 4.**

90 **(A)** Schematic illustration depicting AAV-mediated delivery of GRAB_{NE1h} in the mouse
91 hippocampus and bath application of various agonists in the dentate gyrus.

92 **(B)** Example images showing GRAB_{NE1h} (green) expression and dopamine beta
93 hydroxylase (DBH) immunostaining (red) in the dentate gyrus of AAV-GRAB_{NE1h}- and
94 control-injected hippocampus. The nuclei were counterstained with DAPI. The scale bar
95 represents 100 μm .

96 **(C)** Electrical stimulation evokes NE release in the hippocampus measured as a change in
97 GRAB_{NE1h} fluorescence. The response was blocked by bath application of yohimbine
98 (YO). Exemplar images (**left**), representative traces (**middle**), and the summary data (**right**)
99 are shown.

100 **(D)** Normalized change in GRAB_{NE1h} fluorescence in response to bath application of the
101 indicated noradrenergic agonists in the presence or absence of ICI 118,551 or yohimbine.

102 **(E)** Schematic illustration of the calcium imaging experiments in acute brain slices. The
103 AAVs expressing GRAB_{NE1h} were injected unilaterally into the dentate gyrus and acute
104 brain slices were prepared after 3 weeks and loaded with Cal590 red calcium dye for
105 imaging.

106 **(F)** The fluorescent signal of GRAB_{NE1h} sensor (green) and calcium dye Cal590 (red) in
107 acute brain slices. Scale bar, 20 μm .

108 **(G)** Representative traces of the Cal590 fluorescent response in either a GRAB_{NE1h}-
109 expressing neuron (**upper**) or a non-expressing control neuron (**lower**) to the perfusion of
110 high potassium solution (90mM K⁺).

111 **(H)** The group data of the Cal590 fluorescence responses in GRAB_{NE1h}-expressing
112 neurons or non-expressing control neurons to the perfusion of high potassium solution
113 (n=48 neurons from 7 slices of 3 mice for GRAB_{NE1h}, n=70 neurons from 6 slices of 3 mice
114 for control, p=0.95, student-t test)

115 **(I)** Cumulative plot of the Cal590 fluorescence response. (P=0.93, Kolmogorov-Smirnov
116 test)

117 **(J,K)** Fluorescence responses of GRAB_{NE1m}-expressing cells in an acute LC slice to
118 electrical stimulation of different pulses at 20 Hz in (**J**), or to the exogenous perfusion of
119 different concentrations of NE in (**K**). Left, pseudocolor snapshots of GRAB_{NE1m}
120 fluorescence responses. The white dash circles indicate ROI (50 μm in diameter) used for
121 the fluorescence analysis. Right, corresponding fluorescence responses of left.

122 **(L)** Dose-dependent curve of fluorescence response to different concentrations of NE.
123 Response data were fitted by the Boltzmann equation, and the evoked volume-averaged

124 NE concentration ($[NE]_{vol}$) was estimated based on the calibration curve from the same
125 slice.

126 **(M)** Group data of the evoked $[NE]_{vol}$ during electrical stimulations ($n = 4$ slices from 3
127 mice). Error bars indicate S.E.M.

128 The scale bar shown in **(B)** represents 100 μm . The scale bar shown in **(C)** and **(J)**
129 represent 10 μm .

130 *** $p < 0.001$ (Student's t -test).

131 **Figure S5. GRAB_{NE1h} can sense endogenous NE release and optic tectal neurons**
132 **with or without HuC:GRAB_{NE1m} overexpression show no difference in spontaneous**
133 **calcium responses, related to Figure 5.**

134 **(A,B)** Detection of endogenous NE release in the midbrain of GRAB_{NE1h} zebrafish
135 evoked by visual looming stimuli. Quantification data is shown in **(B)**. n = 6 fish.
136 **(C)** Spontaneous calcium activities of optic tectal neurons revealed by jREGCO1a
137 fluorescent signals show no difference with- or without HuC:GRAB_{NE1m} expression.
138 Experimental diagram is shown in **(C1)**. Traces for representative calcium responses are
139 shown in **(C2)**. Group data are shown in **(C3)**. n = 7 for transgenic HuC:GRAB_{NE1m}
140 zebrafish, and n = 8 for fish without expressing GRAB_{NE1m}.

141

142 * $p < 0.05$ and *** $p < 0.001$; n.s., not significant (Student's *t*-test, Wilcoxon test, or Mann-
143 Whitney rank sum test).

144

145 **Figure S6. No detectable changes in noradrenergic activity are observed in freely**
146 **moving mice after expression of the GRAB_{NEmut} sensor during stress, social**
147 **interactions and food related behaviors, related to Figure 7.**

148 **(A)** Schematic diagrams depicting the AAV virus injection, and recording sites.

149 **(B)** Histology showing the expression of GRAB_{NEmut} (green) and placement of the
150 recording; the nuclei were counterstained with DAPI (blue). Scale bar: 1 mm (left), 500µm
151 (right).

152 **(C1-E5)** Representative traces **(C1-C5)**, average per-stimulus histograms **(D1-D5)**, and
153 summary data **(E1-E5)** showing normalized GRAB_{NE1m} fluorescence ($\Delta F/F$) before and
154 during the forced swim test **(1)**, and before, between and during the tail suspension test
155 **(2)**, the hand presentation test **(3)**, social interaction with an intruder of the opposite sex
156 **(4)**, an intruder of the same sex **(5)** and presentation of peanut butter **(6)**. n = 3 animals
157 each.

158 The Shapiro-Wilk normality test was performed; if the test revealed it followed a normal
159 distribution, a paired Student's *t*-test or one-way repeated measures ANOVA followed by
160 Tukey's multiple comparisons was performed. If the values did not follow a normal
161 distribution, a non-parametric ANOVA (Friedman's test) was performed followed by
162 Dunn's multiple comparisons test. In **(C)** and **(D)**, the blue dotted lines represent the start
163 of the stimulus, and the red dotted lines represent the end of the trial.

164 **p* < 0.05 and ***p* < 0.01.